REPORT DOCUMENTATION PAGE

Form Approved
OMB No. 0704-0188

1. REPORT DATE *(DD-MM-YYYY)*	**2. REPORT TYPE**	**3. DATES COVERED** *(From - To)*
22-10-09	Final Performance	01-06-05 to 05-31-09

4. TITLE AND SUBTITLE
Nonlinear Aspects of Internal Waves in the Atmosphere

5a. CONTRACT NUMBER
05NM038

5b. GRANT NUMBER
FA9550-05-1-0439

5c. PROGRAM ELEMENT NUMBER

6. AUTHOR(S)
John P. McHugh

5d. PROJECT NUMBER

5e. TASK NUMBER

5f. WORK UNIT NUMBER

7. PERFORMING ORGANIZATION NAME(S) AND ADDRESS(ES)

University of New Hampshire
Kingsbury Hall
Durham, NH 03824

8. PERFORMING ORGANIZATION REPORT NUMBER

9. SPONSORING / MONITORING AGENCY NAME(S) AND ADDRESS(ES)
AFOSR/NE
875 N Randolph St, Ste 325
Arlington, VA 22203

10. SPONSOR/MONITOR'S ACRONYM(S)

11. SPONSOR/MONITOR'S REPORT NUMBER(S)
AFRL-OSR-VA-TR-2012-0576

12. DISTRIBUTION / AVAILABILITY STATEMENT

Distribution A: Approved for Public Release

13. SUPPLEMENTARY NOTES

14. ABSTRACT

Internal waves in the atmosphere are responsible for a significant percentage of atmospheric turbulence, particularly at the tropopause. This turbulence can interfere with Air Force operations, and is in need of improved prediction methods. The research has considered a sequence of idealized phenomena aimed at this ultimate goal. The results show that nonlinear effects enhance wave amplitude at the altitude where the buoyancy frequency changes suddenly. Vertically propagating wave packets result in a horizontal mean flow which is due to the wave reflection at by the tropopause. This wave-induced mean flow causes a reduction in the Richardson number both above and below the tropopause, and ultimately forces upwardly propagating waves to overturn and break. Non-Boussinesq effects are important, but must be treated differently than the Boussinesq case to achieve a uniformly valid solution. Simulations of a vortex pair show that the tropopause may act as a boundary for turbulence.

15. SUBJECT TERMS
Waves Nonlinear Atmosphere Flow Stratified Tropopause

16. SECURITY CLASSIFICATION OF: U			**17. LIMITATION OF ABSTRACT**	**18. NUMBER OF PAGES**	**19a. NAME OF RESPONSIBLE PERSON**
a. REPORT	**b. ABSTRACT**	**c. THIS PAGE**	UU		**19b. TELEPHONE NUMBER** *(include area code)*
					(603) 862-1899

John McHugh

Final Report: Nonlinear aspects of internal waves in the atmosphere

John P. McHugh
Department of Mechanical Engineering
University of New Hampshire
Durham, NH 03824
(603) 862-1899
(603) 862-1865 FAX
john.mchugh@unh.edu

20 August 2009

Grant 05NM038, FA9550-05-1-0439

1 Introduction

This document is the final report for project FA 9550-05-1-0439, funded by AFOSR through the DEPSCOR program. The program manager was Arje Nachman. The research was to investigate the dynamics of nonlinear waves and other flows in the vicinity of the tropopause using theoretical and computational methods. The project was very successful, and has resulted in many new and important results. The primary results are documented below.

A number of students in various capacities are now affiliated with the project. They are listed below:

Name	Degree	
Nick Jenkins	MS	
Bob Arredondo	PhD	(part-time)
Surupa Shaw	PhD	
Zhexuan Zhang	PhD	
Imani Lugalla	BS	
Travis Gline	BS	

In addition, Dr. Iordanka Panayotova, previously a postdoc at AFRL at Hanscom, now on the faculty at Old Dominion University, is collaborating with the PI on the theoretical work.

Project funds and matching funds were used for two months of salary for the PI during the summer for 2005, 2006, and 2007, which expended all funds originally allocated for PI salary. Project funds supported two months of salary for the consultant, T. R. Akylas, expending all of this part of the original budget.

A one-year no-cost extension was requested and awarded. This extension of time is necessary due mostly to timing difficulties associated with the graduate students.

2 Boussinesq theory of waves interacting with the tropopause

Waves impinging on an idealized two-layer Boussinesq model of the tropopause region are treated with weakly nonlinear theory. The results have appeared recently in The Journal of Atmospheric Sciences [1].

The waves are assumed to be periodic in the horizontal and propagate with permanent form. Internal waves of permanent form have been treated previously, most notably by Thorpe [30] and Yih [36]. Yih [36] showed that the background density profile must be adjusted to account for a nonlinear shift in the mean streamline. The correction to the background density results in a second-order correction to the wavespeed, analogous to Stokesian waves [28]. However, Yih [36] showed that the correction for internal waves is *negative*, meaning that larger amplitude waves travel slower, opposite to that for free-surface waves. Thorpe [30] and Yih [36] both considered a configuration where the flow is bounded on top by a rigid lid, resulting in complete reflection of the internal waves. The value of correction to the wavespeed depends strongly on the wave reflection. Partial wave reflection occurs in the lower layer of the configuration considered below, also resulting in an important correction to the wavespeed. The present results show that this correction is also negative.

The waves are made steady by choosing a coordinate system that moves horizontally with the wave speed [also used by Stokes [28], Long [17], and Yih [36]]. The governing equations are then reduced to Long's equation [17]. For the case considered here of Boussinesq flow with constant Brunt-Väisälä frequency (in each layer) and no upstream shear, Long's model becomes linear, and is given by

$$\nabla^2 \delta + \kappa^2 \delta = 0, \tag{1}$$

where δ is the vertical displacement of streamlines from an upstream or background state, and κ is a constant. At first glance, it would seem that the solution to the two layer problem considered here is merely the sinusoidal solution

$$\delta \propto \sin mx \sin nz, \tag{2}$$

where m and n are constants unique to each layer. This solution does satisfy (1) exactly, but only meets the boundary conditions at the *mean* interface.

[1] J. McHugh, Journal of the Atmospheric Sciences, **66**, pp. 1845-1855, 2009.

An accurate nonlinear solution must meet the boundary conditions at the actual interfacial position, rather than the mean, which is not known beforehand. As a result, in a multilayer fluid (2) is only a linear solution, accurate for infinitesimal wave amplitudes only. Important nonlinear effects result when the displacement of the interface is included. Further nonlinear effects result when the background density profile is adjusted to match the average density profile in the presence of waves.

It is shown here that the nonlinear effects at the interface result in higher frequency internal waves propagating throughout the fluid. These waves are harmonic to the incident wave only at the interface, where they contribute to steepen the wave. Away from the interface, the harmonics propagate at an angle to the horizontal that is different than the incident wave; the interface causes the harmonics to be scattered. For some parameter values, the linear solution gives an evanescent wave in the upper layer, meaning the vertical structure is not oscillatory. For all parameter values, the higher harmonic waves in both layers become evanescent when the effective frequency is greater than the Brunt-Väisälä frequency.

2.1 Basic equations

The flow is assumed to be incompressible, inviscid, and two-dimensional. Stratification is present due to a non-diffusing quantity. The flow is then governed by the Euler equations, the continuity equation, and the equation of incompressibility. Long [17] reduced these equations to a form now known as Long's model. Long's model assumes a horizontal reference flow, $u_0(z_0)$, with a density profile, $\rho_0(z_0)$, where z_0 is the vertical position in the reference flow. The streamlines may be deflected by a disturbance, often considered to be a barrier to the flow, such as a mountain. The derivation of Long's equation is given by Long [17], and will not be repeated here. The resulting equation is

$$\nabla^2\delta + \frac{1}{2}\frac{1}{q}\frac{dq}{dz}\left[2\frac{\partial\delta}{\partial z} - \left(\nabla\delta\right)^2\right] + \frac{N^2}{u_0^2}\delta = 0, \tag{3}$$

where

$$\delta = z - z_0, \tag{4}$$

is the streamline displacement, and

$$N^2 = -\frac{g}{\rho_0}\frac{\partial\rho_0}{\partial z_0}, \tag{5}$$

$$q = \rho_0 u_0^2. \tag{6}$$

If the Boussinesq approximation is assumed and u_0 is taken to be constant, then Long's equation reduces to

$$\nabla^2 \delta + \frac{g\beta}{u_0^2}\delta = 0, \tag{7}$$

where

$$\beta = -\frac{1}{\rho_0}\frac{\partial \rho_0}{\partial z_0}. \tag{8}$$

The mean density profile is chosen to be continuous, but have a discontinuous first derivative, such that the fluid exists in two semi-infinite layers, each layer having a unique value of the buoyancy frequency. The kinematic interfacial condition is that the normal velocity must be continuous across the interface. The dynamic interfacial condition is that the pressure must be continuous across the interface. As stated by Durran [8], these conditions can be met by choosing δ to obey

$$\delta_1 = \delta_2 \tag{9}$$

and

$$\delta_{1z} = \delta_{2z} \tag{10}$$

at the interface, where δ_1 is the streamline displacement field in the lower layer, and δ_2 for the upper layer. A complete derivation of these conditions is provided in the appendix. Note that these are still the fully nonlinear interfacial conditions, and not just the linear condition. Of course, the condition must still be met on the actual interfacial position, rather than the mean interfacial position, a feature that results in the important nonlinear effects.

The vertical position of the origin of the coordinate system is chosen to be at the mean position of the interface, so that the streamline that corresponds to the interface is given by $z_0 = 0$. The displacement of the interface is then determined by

$$\delta\big(x, z\big) = z. \tag{11}$$

Inverting this expression to obtain the interfacial shape, even for relatively simple expressions for δ, is nontrivial. Assume such a solution to (11) is

$$z = \eta\big(x\big). \tag{12}$$

Note that $\delta\big(x,0\big)$ is not the same as $\eta\big(x\big)$, except in the linear case. The interfacial displacement, η, is related to the velocity field by the familiar kinematic interfacial condition for each layer:

$$\eta_t + \big(1-\delta_z\big)\eta_x = \delta_x \tag{13}$$

on the interface.

Expand (9), (10), and (13) in a Taylor series about the mean position of the interface, and insert into the interfacial conditions to obtain

$$\delta_1\Big|_{z=0} + \delta_{1z}\Big|_{z=0}\eta + \frac{1}{2}\delta_{1zz}\Big|_{z=0}\eta^2 + \cdots = \delta_2\Big|_{z=0} + \delta_{2z}\Big|_{z=0}\eta + \frac{1}{2}\delta_{2zz}\Big|_{z=0}\eta^2 + \cdots \tag{14}$$

$$\delta_{1z}\Big|_{z=0} + \delta_{1zz}\Big|_{z=0}\eta + \frac{1}{2}\delta_{1zzz}\Big|_{z=0}\eta^2 + \cdots = \delta_{2z}\Big|_{z=0} + \delta_{2zz}\Big|_{z=0}\eta + \frac{1}{2}\delta_{2zzz}\Big|_{z=0}\eta^2 + \cdots \tag{15}$$

$$\eta_t + \left(1 - \left[\delta_{1z}\Big|_{z=0} + \delta_{1zz}\Big|_{z=0}\eta + \cdots\right]\right)\eta_x = \left(\delta_{1x}\Big|_{z=0} + \delta_{1xz}\Big|_{z=0}\eta + \cdots\right) \tag{16}$$

$$\eta_t + \left(1 - \left[\delta_{2z}\Big|_{z=0} + \delta_{2zz}\Big|_{z=0}\eta + \cdots\right]\right)\eta_x = \left(\delta_{2x}\Big|_{z=0} + \delta_{2xz}\Big|_{z=0}\eta + \cdots\right) \tag{17}$$

2.2 Finite amplitude waves

The governing equation in each layer is the linear Long's equation,

$$\nabla^2\delta_1 + \frac{g\beta_1}{u_1^2}\delta_1 = 0, \tag{18}$$

$$\nabla^2\delta_2 + \frac{g\beta_2}{u_2^2}\delta_2 = 0, \tag{19}$$

where u_1 and u_2 are background velocities for each layer. Expand δ in a power series in ϵ, the ratio of the wave amplitude to horizontal wavelength:

$$\delta_1 = \epsilon\delta_{11} + \epsilon^2\delta_{12} + \epsilon^3\delta_{13} + \cdots, \tag{20}$$

and similar expressions for δ_2 and η. Note the subscript convention; the first index indicates the layer, while the second indicates the order.

A coordinate system is chosen to be moving with the wavespeed (as yet undetermined) to make the flow steady, and the wavespeed must also be

expanded in the wave amplitude to suppress secular terms. Both features are treated with

$$u_1 = c_{10}\left[1 + \epsilon c_{11} + \epsilon^2 c_{12} + \cdots\right]. \tag{21}$$

$$u_2 = c_{20}\left[1 + \epsilon c_{21} + \epsilon^2 c_{22} + \cdots\right]. \tag{22}$$

Ultimately, u_1 and u_2 must be equal to the wavespeed and to each other, so that the flow is steady. However it is convenient to maintain them separately for now, and then ultimately equate them to determine the wavenumber in the upper layer.

To expedite the correction to the background density profile, β is also expanded in the wave amplitude:

$$\beta_1 = \beta_{10}\left[1 + \epsilon\beta_{11} + \epsilon^2\beta_{12}\cdots\right], \tag{23}$$

and a similar expression for β_2.

The first order governing equations are

$$\nabla^2\delta_{11} + \frac{g\beta_{10}}{c_{10}^2}\delta_{11} = 0, \tag{24}$$

$$\nabla^2\delta_{21} + \frac{g\beta_{20}}{c_{20}^2}\delta_{21} = 0, \tag{25}$$

and the interfacial conditions are

$$\delta_{11} = \delta_{21}, \tag{26}$$

$$\delta_{11z} = \delta_{21z} \tag{27}$$

$$\eta_{1x} = \delta_{11x} = \delta_{21x}, \tag{28}$$

on $z = 0$.

The solution to (24-28) is chosen to be an upwardly propagating incident wave in the bottom layer. The linear interfacial conditions require a reflected in the lower layer and a transmitting wave in the upper layer:

$$\begin{aligned}\delta_{11} &= Ae^{imx}\left[e^{-in_1 z} + \left(\frac{n_1 - n_2}{n_1 + n_2}\right)e^{in_1 z}\right] \\ &\quad + A^* e^{-imx}\left[e^{in_1 z} + \left(\frac{n_1 - n_2}{n_1 + n_2}\right)e^{-in_1 z}\right]\end{aligned} \tag{29}$$

$$\delta_{21} = \left(\frac{2n_1}{n_1+n_2}\right)\left[Ae^{i\left(mx-n_2z\right)} + A^*e^{-i\left(mx-n_2z\right)}\right], \tag{30}$$

where n_1 and n_2 are the vertical wavenumbers in the lower and upper layers, respectively, and A^* is the complex conjugate of A. Note that (29) and (30) are chosen to satisfy a radiation condition in each layer.

The corresponding displacement of the interface is

$$\eta_1 = \left[\frac{2n_1}{n_1+n_2}\right]\left[Ae^{imx} - A^*e^{-imx}\right]. \tag{31}$$

The dispersion relations are

$$c_{10}^2 = \frac{g\beta_{10}}{m^2+n_1^2}, \tag{32}$$

$$c_{20}^2 = \frac{g\beta_{20}}{m^2+n_2^2}. \tag{33}$$

The dispersion relation for the upper layer must give the same wave speed, and share the same horizontal wavenumber, m, as the lower layer, which determines the vertical wavenumber in the upper layer. The first approximation to this vertical wavenumber is

$$n_2^2 = m^2\left[\frac{\beta_{20}}{\beta_{10}} - 1\right] + n_1^2\frac{\beta_{20}}{\beta_{10}}. \tag{34}$$

2.2.1 Second order

The second-order governing equations are

$$\nabla^2\delta_{12} + \frac{g\beta_{10}}{c_{10}^2}\delta_{12} = -2c_{11}\nabla^2\delta_{11} - \frac{g\beta_{11}}{c_{10}^2}\delta_{11}, \tag{35}$$

$$\nabla^2\delta_{22} + \frac{g\beta_{20}}{c_{10}^2}\delta_{22} = -2c_{21}\nabla^2\delta_{21} - \frac{g\beta_{21}}{c_{20}^2}\delta_{21}, \tag{36}$$

Before proceeding further, the correction to the upstream condition must be considered to determine β_{11} and β_{21}. This is achieved as described in the next section. The analysis shows that there is no correction at this order, matching the conclusions of Yih [36], and the details will not be given:

$$\beta_{11} = \beta_{21} = 0. \tag{37}$$

The only secular term left in (24) and (25) is suppressed by choosing $c_{11} = c_{21} = 0$, making the second order equations homogeneous.

The second-order interfacial conditions are

$$\delta_{12} - \delta_{22} = \Big[\delta_{21z} - \delta_{11z}\Big]\eta_1, \tag{38}$$

$$\delta_{12z} - \delta_{22z} = \Big[\delta_{21zz} - \delta_{11zz}\Big]\eta_1, \tag{39}$$

$$\eta_{2x} - \delta_{12x} = \frac{\partial}{\partial x}\Big(\delta_{11z}\eta_1\Big), \tag{40}$$

$$\eta_{2x} - \delta_{22x} = \frac{\partial}{\partial x}\Big(\delta_{21z}\eta_1\Big), \tag{41}$$

on $z = 0$. Using (27) reduces (38) to

$$\delta_{12} - \delta_{22} = 0, \tag{42}$$

on $z = 0$. Inserting (29), (30), and (31) into (39) then simplifying gives

$$\delta_{12z} - \delta_{22z} = \left[\frac{2n_1}{n_1 + n_2}\right]^2 \Big(n_1^2 - n_2^2\Big)\Big[A^2 e^{i2mx} + A^{*2} e^{-i2mx} + 2AA^*\Big] \tag{43}$$

on $z = 0$. The forcing terms in (43) are not resonant, and require a solution of the form

$$\delta_{12} = B\sin(2mx + n_{12}z) + C\sin(\gamma_{12}z), \tag{44}$$

where B and C still need to be determined. The vertical wavenumber in (44), n_{12}, is not determined by the interfacial conditions, and is chosen to satisfy the governing equations in the bottom layer, reflected in the dispersion relation for the bottom layer:

$$n_{12}^2 = n_1^2 - 3m^2. \tag{45}$$

The term $C\sin(\gamma_{12}z)$ balances the constant in (43), and represents a wave-induced mean flow, but driven by the interfacial conditions. The governing equation determines the exponent:

$$\gamma_{12}^2 = \frac{g\beta_{10}}{c_{10}^2} = m^2 + n_1^2. \tag{46}$$

Similarly in the upper layer,

$$\delta_{22} = B\sin(2mx - n_{22}z) + C\sin(\gamma_{22}z), \tag{47}$$

$$n_{22}^2 = n_2^2 - 3m^2, \tag{48}$$

$$\gamma_{22}^2 = \frac{g\beta_{20}}{c_{20}^2}, \tag{49}$$

where the coefficients have already been chosen to satisfy (42). Note that the negative sign in front of n_{22} is chosen in the upper layer to obtain an upwardly propagating harmonic, meeting the radiation condition at the top.

Equation (39) determines B and C:

$$B = -4n_1^2\frac{n_1 - n_2}{n_1 + n_2}A^2, \tag{50}$$

$$C = \left[\frac{2n_1}{n_1 + n_2}\right]^2 \frac{n_1^2 - n_2^2}{\gamma_{12} + \gamma_{22}} 2AA^*. \tag{51}$$

2.2.2 Correction to β

The second-order solution must match the background conditions. This is achieved using the method of Yih [36]. The definition of δ is rearranged to obtain

$$z = z_0 + \delta\Big(x, z\Big). \tag{52}$$

The inversion of this equation is

$$z = \eta\Big(x, \rho\Big). \tag{53}$$

An average over one wave period of (53) is the average displacement of a line of constant density in the presence of waves. A wave of permanent form must have this vertical displacement equal to zero. If it is not, then the upstream density profile must be adjusted. This adjustment is determined using

$$\frac{1}{\rho_0}\frac{d\rho}{dz_0} = \frac{1}{\rho_0}\frac{d\rho}{d\overline{\eta}}\frac{d\overline{\eta}}{dz_0} = -\beta\frac{d\overline{\eta}}{dz_0}. \tag{54}$$

In practice, (52) is inverted using the method of successive approximations for each layer, as in Yih [36] and Stokes [28]. The final result is

$$\beta_{21} = 4AA^*n_1^2\left(\frac{n_1 - n_2}{n_1 + n_2}\right)\left(\frac{\gamma_{12}}{\gamma_{12} + \gamma_{22}}\cos\gamma_{12}z_0 - 2\cos 2n_1 z_0\right), \tag{55}$$

$$\beta_{22} = 0. \tag{56}$$

Note that the correction for the upper layer is zero because there is no reflection, only the incident wave. The correction for the lower layer is non-zero because of the interaction between the incident wave and its reflection from the interface.

2.2.3 Third order

The third-order solution is pursued just far enough to demonstrate uniform validity, and thereby determine the second-order correction to the wavespeed. The third-order governing equations are

$$\nabla^2\delta_{13} + \frac{g\beta_{10}}{c_0^2}\delta_{13} = -2c_{12}\nabla^2\delta_{11} - \frac{g\beta_{12}}{c_{10}^2}\delta_{11}, \tag{57}$$

$$\nabla^2\delta_{23} + \frac{g\beta_{20}}{c_0^2}\delta_{23} = -2c_{22}\nabla^2\delta_{21} - \frac{g\beta_{22}}{c_{20}^2}\delta_{21}. \tag{58}$$

The third-order interfacial conditions are

$$\delta_{13} - \delta_{23} = \Big[\delta_{21z} - \delta_{11z}\Big]\eta_2 + \Big[\delta_{22z} - \delta_{12z}\Big]\eta_1 + \frac{1}{2}\Big[\delta_{21zz} - \delta_{11zz}\Big]\eta_1^2, \tag{59}$$

$$\delta_{13z} - \delta_{23z} = \Big[\delta_{21zz} - \delta_{11zz}\Big]\eta_2 + \Big[\delta_{22zz} - \delta_{12zz}\Big]\eta_1 + \frac{1}{2}\Big[\delta_{21zzz} - \delta_{11zzz}\Big]\eta_1^2, \tag{60}$$

$$\eta_{3t} + \eta_{3x} - \delta_{13x} = \frac{\partial}{\partial x}\left(\delta_{11z}\eta_2 + \delta_{12z}\eta_1 + \frac{1}{2}\delta_{11zz}\eta_1^2\right), \tag{61}$$

$$\eta_{3t} + \eta_{3x} - \delta_{23x} = \frac{\partial}{\partial x}\left(\delta_{21z}\eta_2 + \delta_{22z}\eta_1 + \frac{1}{2}\delta_{21zz}\eta_1^2\right) \tag{62}$$

on $z = 0$.

The forcing terms in the interfacial conditions are not resonant, nor will they be at any order, and hence they do not contribute to the second-order correction to the wave-speed. This is because the wave speed is not determined by the interfacial conditions, as interfacial waves do not exist when the density is continuous. The interfacial forcing terms are still important however, as they result in scattered harmonics of the incident waves, discussed in the next section.

The forcing terms in the governing equation for the lower layer are secular, as a result of the nonzero value of β_{12}. These terms are suppressed, again

following Yih [36], by multiplication with the expression for δ_1 in the lower layer, and integration over a single wave period. The resulting second-order correction to the wavespeed in the lower layer is

$$c_{12} = 2n_1^2 AA^* \Bigg\{ \left(\frac{n_1 - n_2}{n_1 + n_2}\right)\left(\frac{1}{\gamma_{12} + \gamma_{22}}\right)\frac{\sin\frac{2\pi\gamma_{12}}{n_1}}{\frac{2\pi}{n_1}} + \frac{1}{2}\left(\frac{(n_1 - n_2)^2}{n_1^2 + n_2^2}\right)\left(\frac{\gamma_{12}}{\gamma_{12} + \gamma_{22}}\right)\Bigg[-2 + \left(\frac{1}{2n_1 - \gamma_{12}}\right)\frac{\sin(2n_1 - \gamma_{12})\frac{2\pi}{n_1}}{\frac{2\pi}{n_1}} + \left(\frac{1}{2n_1 + \gamma_{12}}\right)\frac{\sin(2n_1 + \gamma_{12})\frac{2\pi}{n_1}}{\frac{2\pi}{n_1}}\Bigg]\Bigg\}, \quad (63)$$

while for the upper layer,

$$c_{22} = 0. \quad (64)$$

The final stage is to determine n_2, governed by the equality of wave-speeds in the two layers. Setting $u_1 = u_2$ in (21) and (22) and keeping terms to second order results in

$$\frac{g\beta_{10}}{m^2 + n_1^2}\left[1 + \epsilon^2 c_{12}\right] = \frac{g\beta_{20}}{m^2 + n_2^2} \quad (65)$$

This expression along with (63) represents two coupled algebraic expressions for n_2 and c_{12}, which are determined numerically.

2.3 Discussion

Internal waves only exist for frequencies that are less than the buoyancy frequency, $N = g\beta$, as can be shown from the dispersion relation. Hence the incident waves in the lower layer must have a frequency less than $g\beta_{10}$. The buoyancy frequency above the interface may be larger or smaller than below: the buoyancy frequency at the tropopause and the mesopause increases with the vertical coordinate, while the buoyancy frequency at the stratopause decreases.

For the case where $N_2 < N_1$ (the stratopause), it is possible for the frequency of the linear incident wave to be greater than N_2. The linear transmitted wave will be evanescent in the upper layer, with no vertical oscillations in the upper layer.

For the case where $N_2 > N_1$ (the tropopause and mesopause), the linear incident wave creates a wave in the upper layer that oscillates with the vertical. However, the harmonics that are created at the interface may be evanescent in either layer. The harmonic may be considered to have an effective frequency; for example, the second harmonic in the lower layer would have the effective frequency,

$$\left(\frac{2m}{\sqrt{(2m)^2 + n_{12}^2}} \right) N_1. \tag{66}$$

If the effective frequency of a harmonic is greater than the Brunt-Väisälä frequency in either layer, then the harmonic will be evanescent in that layer. This transition occurs when the vertical wavenumber becomes purely imaginary, for example, if $n_{12}^2 > 0$ in (45), then n_{12} is real and the harmonic is oscillatory. If $n_{12}^2 < 0$, then the behavior is evanescent.

Away from the interface, the higher harmonics with vertical oscillation will not coincide with the primary mode. For example, the incident waves in the lower layer are traveling waves with wavenumbers m and n_1, as discussed previously. The lines of constant phase for this wave make an angle, θ_1, to the horizontal:

$$\theta_1 = \arccos \frac{m}{\sqrt{m^2 + n_1^2}}. \tag{67}$$

The second-order solution requires a harmonic with wavenumbers $2m$ and n_{12}, where n_{12} is given by (45). This harmonic is a wave that makes an angle, θ_{12}, with the horizontal:

$$\theta_{12} = \arccos \frac{2m}{\sqrt{(2m)^2 + n_{12}^2}} = \arccos \frac{2m}{\sqrt{m^2 + n_1^2}}, \tag{68}$$

where (45) has been used to simplify (68). Clearly, the angle of the incident wave is different than the angle of the second-order harmonic wave; the second-order harmonic has been scattered by the interface.

The third-order interfacial conditions will result in third-order harmonics with a higher effective frequency than the second-order harmonic. Depending on the parameter values of the incident wave, this frequency could be greater than the buoyancy frequency in either layer, resulting in non-oscillatory behavior, and an evanescent mode. Furthermore, eventually there is a harmonic in the Stokes expansion that will result in a harmonic frequency that is greater than both N_1 and N_2, and this harmonic will be evanescent in both layers, as will all higher harmonics.

The deflection of the interface due to the second-order harmonics has the same phase as the deflection of the interface due to the linear waves given by (31), whether the harmonic is oscillatory or not. The third-order harmonic will also have this phase. As a result, the nonlinear wave at the tropopause behaves as a Stokes wave, where the crest is sharpened and the trough broadened.

However, the behavior of the waves away from the interface is significantly different. Only the oscillatory harmonics extend away from the interface, and depending on the wavenumbers for the incident wave, only the first few harmonics are likely to be oscillatory. The remainder of the harmonics will decay exponentially in each layer. Hence a horizontal profile would consist of the sum of only a few sinusoidal components, quite different than the behavior at the interface.

The second-order correction to the wave-speed and the wavenumber in the upper layer are determined by the two coupled nonlinear algebraic equations given in (63) and (65). Values of c_{12} and n_2 have been determined numerically using the bisection method, and are shown in figures 2.3 and 2.3. Figure 2.3 shows that c_{12} is negative, meaning that larger amplitude waves travel *slower* than infinitesimal waves. This result was demonstrated by Yih [36] for internal waves bounded with rigid horizontal surfaces. The rigid surfaces in Yih [36] cause complete wave reflection, which in turn leads to a non-zero wave-induced mean flow and a displacement of isopycnic lines. The present results have partial wave reflection from the interface, rather than the complete reflection as in Yih [36]. Furthermore, there is an additional contribution to the wave-induced mean flow as a result of the interfacial conditions, given by the second term in (44). This interfacial mean flow weakens the effect, but is not significant enough to overcome the effect found by Yih [36], and hence the same mechanism that results in the negative wavespeed correction is also at work here.

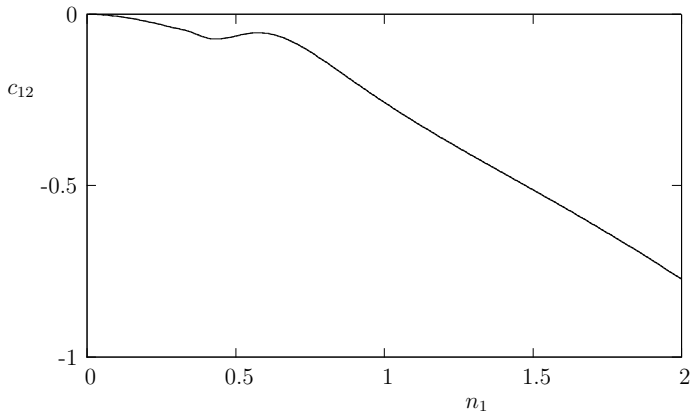

Figure 1: Wave speed correction

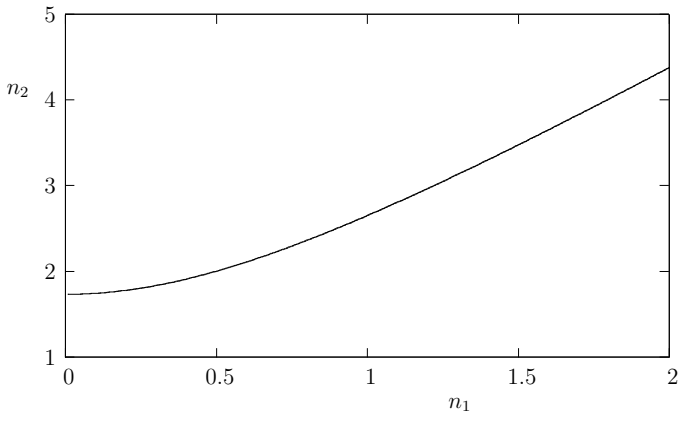

Figure 2: Wavenumber in the upper layer

3 DNS of waves at the tropopause

The direct numerical simulation (DNS) of waves interacting with an idealized tropopause was treated for a variety of conditions. Waves are created beneath the interface and allowed to impinge on the interface. The results show that a horizontal mean flow is created at the interface that grows in strength and finally creates a critical layer. These results have been published in Theoretical and Computational Fluid Dynamics [2].

3.1 Governing equations

The governing equations are the anelastic equations [16, 19, 34]. The anelastic equations are an approximate form of the Navier-Stokes equations where the effects of sound wave propagation have been removed. The original anelastic equations are flawed, and the linear solution does not match the linear solution of the fully compressible equations. It was later shown that the pressure term was incorrect. Bacmeister and Schoeberl [4] provide a concise derivation of the corrected anelastic equations, which have been found to accurately model atmospheric dynamics.

For large-scale waves typically found in the atmosphere, viscosity is not important; inviscid flow is asssumed here. The inviscid anelastic equations in two dimensions for a perfect gas atmosphere are

$$\frac{Du}{Dt} = -\frac{\partial p^*}{\partial x}, \tag{69}$$

$$\frac{Dw}{Dt} = -\frac{\partial p^*}{\partial z} + g\frac{\theta}{\overline{\theta}}, \tag{70}$$

$$\frac{D\theta}{Dt} + w\frac{\partial \overline{\theta}}{\partial z} = 0, \tag{71}$$

$$\frac{\partial \overline{\rho} u}{\partial x} + \frac{\partial \overline{\rho} v}{\partial y} = 0, \tag{72}$$

where

$$p^* = c_p \overline{\theta} \left(\frac{p}{p_0} \right)^{\frac{R}{c_p}}, \tag{73}$$

$$\frac{D}{Dt} = \frac{\partial}{\partial t} + u\frac{\partial}{\partial x} + w\frac{\partial}{\partial z}, \tag{74}$$

[2] McHugh, J. P., Theoretical and Computational Fluid Dynamics, **22**, pp107-123, 2008.

u, w are the velocity components, x, z are the components of position, θ is the potential temperature, $\overline{\rho}$ and $\overline{\theta}$ are the base state density and potential temperature, respectively, c_p is the specific heat at constant pressure, R is the gas constant, g is the gravitational constant, p is the pressure, and p_0 is a constant. Equations (69-70) are the momentum equations, (71) is the energy equation, and (72) is the continuity equation.

3.2 The base state

The base state is governed by the perfect gas law,

$$\overline{p} = \overline{\rho} R \overline{T}, \tag{75}$$

and the equation of static equilibrium,

$$\frac{d\overline{p}}{dz} = -\overline{\rho} g. \tag{76}$$

Note that all base state variables are denoted by an overline. An important base-state parameter is the Brunt-Väisälä frequency, defined as

$$N^2 = \frac{g}{\overline{\theta}} \frac{d\overline{\theta}}{dz}. \tag{77}$$

A variety of base states may be considered, including cases drawn from observations. However, the base state must satisfy the above base state equations to be valid. Often the base state temperature is chosen, and then the density and potential temperature are determined. The following two relations, which are derived directly from the first law of thermodynamics for a dry atmosphere and the definition of potential temperature [13], are used to determine $\overline{\rho}$ and $\overline{\theta}$ once $\overline{T}$ is chosen:

$$\frac{\overline{\rho}_z}{\overline{\rho}} + \frac{\overline{T}_z}{\overline{T}} + \frac{g}{R\overline{T}} = 0, \tag{78}$$

$$\frac{\overline{\theta}_z}{\overline{\theta}} - \frac{\overline{T}_z}{\overline{T}} - \frac{g}{c_p \overline{T}} = 0. \tag{79}$$

The base-state temperature for the present results is chosen to be constant in each layer, making the Brunt-Väisälä frequency constant and equal to $\frac{g^2}{c_p \overline{T}}$, with a unique value in each layer. The potential temperature is given by

$$\overline{\theta} = e^{\frac{gz}{c_p \overline{T}}}, \tag{80}$$

where the exponent has a unique value in each layer. The pressure must be continuous at the interface for equilibrium, and density is chosen to be continuous. The potential temperature is also chosen to be continuous at the interface.

Another important base state parameter is the scale height, H, which is the thickness of a layer of gas of constant temperature over which the density changes by the factor, e. The local value of the scale height is defined by

$$\frac{1}{H} = -\frac{\overline{\rho}_z}{\overline{\rho}}. \tag{81}$$

For a constant temperature layer, the scale height is given by $H = \frac{R\overline{T}}{g}$. The above choices result in a constant scale height throughout the domain.

3.3 The computational approach

The velocity, position, and pressure are rescaled using a length scale, L, and a velocity scale, U. The wave forcing is chosen to have a horizontal wavelength, λ, that is equal to the horizontal length of the domain, and this lengthscale is chosen as the lengthscale for rescaling; $L = \lambda$. The flow is initiated from rest; the initial mean flow is also zero. This means that the basic state does not provide a natural velocity scale. Instead, the velocity scale is chosen to be $\sqrt{\lambda g}$. The density and potential temperature are rescaled using their respective base-state values at the bottom of the domain ($\overline{\rho_0}$, $\overline{\theta_0}$). The dimensionless equations are

$$\frac{D\tilde{u}}{D\tilde{t}} = -\frac{\partial \tilde{p}}{\partial \tilde{x}}, \tag{82}$$

$$\frac{D\tilde{w}}{D\tilde{t}} = -\frac{\partial \tilde{p}}{\partial \tilde{z}} + \frac{\tilde{\theta}}{\tilde{\overline{\theta}}}, \tag{83}$$

$$\frac{D\tilde{\theta}}{D\tilde{t}} + \tilde{w}\frac{\partial \tilde{\overline{\theta}}}{\partial \tilde{z}} = 0, \tag{84}$$

$$\frac{\partial \tilde{\overline{\rho}}\tilde{u}}{\partial \tilde{x}} + \frac{\partial \tilde{\overline{\rho}}\tilde{v}}{\partial \tilde{y}} = 0, \tag{85}$$

where the circumflex denotes a dimensionless quantity.

The governing equations are reduced such that the pressure, horizontal velocity, and potential temperature are eliminated from the linear terms, resulting in

$$\frac{\partial^2}{\partial \tilde{t}^2}\left[\nabla^2\tilde{w} + \frac{\partial}{\partial \tilde{z}}\left(\frac{1}{\tilde{H}}\tilde{w}\right)\right] + \tilde{N}^2\nabla_1^2\tilde{w} = \frac{\partial}{\partial \tilde{t}}\left[\frac{\partial}{\partial \tilde{z}}\frac{\partial \tilde{A}_i}{\partial \tilde{x}_i} - \nabla^2\tilde{A}_3\right] - \nabla_1^2\left[\frac{\tilde{B}}{\tilde{\bar{\theta}}}\right], \tag{86}$$

where the $\tilde{A}_i$ is the sum of the nonlinear terms for the i^{th} momentum equation,

$$\tilde{A}_i = \tilde{u}_j\frac{\partial \tilde{u}_i}{\tilde{x}_j}, \tag{87}$$

$\tilde{B}$ is the sum of the nonlinear terms for the energy equation,

$$\tilde{B} = \tilde{u}_j\frac{\partial \tilde{\theta}}{\tilde{x}_j}, \tag{88}$$

and

$$\nabla_1^2 = \frac{\partial^2}{\partial \tilde{x}^2}. \tag{89}$$

The boundary condition on the top boundary, $\tilde{z} = \frac{D}{L}$, where D is the height of the domain, is $\tilde{w} = 0$. Note that a damping layer is included near the top boundary to absorb upward propagating waves, as will be discussed later. On the bottom boundary, $\tilde{w}$ is the imposed forcing velocity, also discussed later. The side boundaries are treated as periodic.

The order of (86) is reduced by introducing $\tilde{\phi}$:

$$\tilde{\phi} = \frac{\partial}{\partial \tilde{t}}\left[\nabla^2\tilde{w} + \frac{\partial}{\partial \tilde{z}}\left(\frac{1}{\tilde{H}}\tilde{w}\right)\right] - \left[\frac{\partial}{\partial \tilde{z}}\frac{\partial \tilde{A}_i}{\partial \tilde{x}_i} - \nabla^2\tilde{A}_3\right]. \tag{90}$$

Equation (86) becomes

$$\frac{\partial \phi}{\partial \tilde{t}} + \tilde{N}^2\nabla_1^2\tilde{w} = -\nabla_1^2\left[\frac{\tilde{B}}{\tilde{\bar{\theta}}}\right]. \tag{91}$$

The variable $\tilde{\phi}$ is retained in the calculations, and $\tilde{w}$ and $\tilde{\phi}$ are determined, using (90) and (91), for each time step. Note that the nonlinear terms that contain a temporal derivative have been carefully chosen as part of the definition of $\tilde{\phi}$. This subtle but important step allows the nonlinear terms to

be evaluated by accurate well-known methods, such as Adams-Bashforth, to any level of accuracy.

Equation (90) and (91), being first-order in time, may be directly integrated over the time step, $\Delta\tilde{t}$, to obtain

$$\left[\nabla^2\tilde{w}+\frac{\partial}{\partial\tilde{z}}\left(\frac{1}{\tilde{H}}\tilde{w}\right)\right]^{n+1}-\left[\nabla^2\tilde{w}+\frac{\partial}{\partial\tilde{z}}\left(\frac{1}{\tilde{H}}\tilde{w}\right)\right]^{n}+\int_{\tilde{t}^n}^{\tilde{t}^{n+1}}\tilde{\phi}\,d\tilde{t}= -\int_{\tilde{t}^n}^{\tilde{t}^{n+1}}\left[\frac{\partial}{\partial\tilde{z}}\frac{\partial\tilde{A}_i}{\partial\tilde{x}_i}-\nabla^2\tilde{A}_3\right]d\tilde{t}, \quad (92)$$

$$\tilde{\phi}^{n+1}-\tilde{\phi}^{n}+\int_{\tilde{t}^n}^{\tilde{t}^{n+1}}\tilde{N}^2\nabla_1^2\tilde{w}\,d\tilde{t}=-\int_{\tilde{t}^n}^{\tilde{t}^{n+1}}\nabla_1^2\left[\frac{\tilde{B}}{\tilde{\bar{\theta}}}\right]d\tilde{t}. \quad (93)$$

The integrals in the linear terms in (92) and (93) are treated implicitly with the Crank-Nicolson method, while the nonlinear terms are treated explicitly with the second-order Adams-Bashforth method. The result is

$$\left[\nabla^2\tilde{w}+\frac{\partial}{\partial\tilde{z}}\left(\frac{1}{\tilde{H}}\tilde{w}\right)\right]^{n+1}-\left[\nabla^2\tilde{w}+\frac{\partial}{\partial\tilde{z}}\left(\frac{1}{\tilde{H}}\tilde{w}\right)\right]^{n}+\left[\frac{\tilde{\phi}^{n+1}+\tilde{\phi}^{n}}{2}\right]\Delta\tilde{t}= \frac{1}{2}\left[3\left(\frac{\partial}{\partial\tilde{z}}\frac{\partial\tilde{A}_i}{\partial\tilde{x}_i}-\nabla^2\tilde{A}_3\right)^{n}-\left(\frac{\partial}{\partial\tilde{z}}\frac{\partial\tilde{A}_i}{\partial\tilde{x}_i}-\nabla^2\tilde{A}_3\right)^{n-1}\right]\Delta\tilde{t}, \quad (94)$$

$$\tilde{\phi}^{n+1}-\tilde{\phi}^{n}+\tilde{N}^2\nabla_1^2\left[\frac{\tilde{w}^{n+1}+\tilde{w}^{n}}{2}\right]\Delta\tilde{t}=-\frac{1}{\tilde{\bar{\theta}}}\nabla_1^2\left[\frac{3\tilde{B}^{n}-\tilde{B}^{n-1}}{2}\right]\Delta\tilde{t}. \quad (95)$$

There is one remaining difficulty; both equations contain $\tilde{w}$ and $\tilde{\phi}$ at the leading time step, making them coupled. The two equations may be decoupled merely by eliminating $\tilde{\phi}^{n+1}$ algebraically, resulting in

$$\left[\nabla^2\tilde{w}+\frac{\partial}{\partial\tilde{z}}\left(\frac{1}{\tilde{H}}\tilde{w}\right)\right]^{n+1}-\frac{\Delta\tilde{t}^2}{4}\tilde{N}^2\nabla_1^2\tilde{w}^{n+1}= \left[\nabla^2\tilde{w}+\frac{\partial}{\partial\tilde{z}}\left(\frac{1}{\tilde{H}}\tilde{w}\right)\right]^{n}+\frac{\Delta\tilde{t}^2}{4}\tilde{N}^2\nabla_1^2\tilde{w}^{n}+\Delta\,\tilde{t}\tilde{\phi}^{n} +\frac{\Delta\tilde{t}}{2}\left[3\left(\frac{\partial}{\partial\tilde{z}}\frac{\partial\tilde{A}_i}{\partial\tilde{x}_i}-\nabla^2\tilde{A}_3\right)^{n}-\left(\frac{\partial}{\partial\tilde{z}}\frac{\partial\tilde{A}_i}{\partial\tilde{x}_i}-\nabla^2\tilde{A}_3\right)^{n-1}\right] -\frac{\Delta\tilde{t}^2}{4}\frac{1}{\tilde{\bar{\theta}}}\nabla_1^2\left(3\tilde{B}^{n}-\tilde{B}^{n-1}\right). \quad (96)$$

Equation (96) may be solved directly for $\tilde{w}^{n+1}$. Values of $\tilde{\phi}^{n+1}$ may then be determined using either (94) or (95); (95) is used in practice for efficiency.

The continuity equation is used to determine the horizontal velocity:

$$\tilde{u}_{\tilde{x}} = -\left[\tilde{w}_{\tilde{z}} + \frac{\tilde{\bar{\rho}}_{\tilde{z}}}{\tilde{\bar{\rho}}}\tilde{w}\right]. \tag{97}$$

This equation is easily solved for $\tilde{u}^{n+1}$ once $\tilde{w}^{n+1}$ is available. That leaves only $\tilde{\theta}$, which can be found directly from the energy equation,

$$\tilde{\theta}^{n+1} - \tilde{\theta}^{n} = -\frac{\partial\tilde{\bar{\theta}}}{\partial\tilde{z}}\left[\frac{\tilde{w}^{n+1}+\tilde{w}^{n}}{2}\right]\Delta\tilde{t} - \left[\frac{3\tilde{B}^{n}-\tilde{B}^{n-1}}{2}\right]\Delta\tilde{t}. \tag{98}$$

The continuity equation cannot be used to determine the horizontal average of horizontal velocity, $\langle\tilde{u}\rangle$, where the angle brackets indicate the horizontal average, since any profile of $\langle\tilde{u}\rangle$ will satisfy continuity. Instead the horizontal average of the horizontal momentum equation is used:

$$\frac{\partial\langle\tilde{u}\rangle}{\partial\tilde{t}} = -\frac{1}{\tilde{\bar{\rho}}}\frac{\partial}{\partial\tilde{z}}\langle\tilde{\bar{\rho}}\tilde{u}\tilde{w}\rangle. \tag{99}$$

Note that the above formulation is easily extended to three dimensions.

The spatial discretization is a spectral method. The horizontal direction is expanded in a Fourier series. The vertical direction uses an expansion in Cardinal functions, collocated on the Chebyshev-Gauss-Lobatto grid. Details of this spatial method can be found in Solomonoff and Turkel [27] and Boyd [6]. Matrix equations are treated with direct methods.

Note that N is discontinous at the interface, which is sometimes incompatible with a spectal method, leading to Gibbs type oscillations. For the present method, since the spatial treatment is collocation, the actual value of N at each gridpoint is used directly in the discrete equations. The resulting solution for w^{n+1} in (94) is continuous, even though N is discontinuous, hence Gibbs oscillations do not appear.

Waves are forced by imposing an artificial vertical velocity at the bottom of the domain. The imposed frequency and amplitude determine the character of the resulting wavetrain. The forcing creates a wave packet with finite vertical extent. The envelope function is the raised cosine. This bottom forcing is given by

$$\tilde{w}(0,\tilde{x},\tilde{t}) = \begin{cases} \frac{1}{2}\tilde{\alpha}\left[1-\cos\left(\frac{2\pi\tilde{t}}{j\tilde{T}}\right)\right]\sin\left(\tilde{x}-\tilde{\sigma}\tilde{t}\right) & \text{if } \tilde{t} < j\tilde{T} \\ 0 & \text{if } \tilde{t} > j\tilde{T}, \end{cases} \tag{100}$$

where $\tilde{\sigma}$ is the forcing frequency, $\tilde{\alpha}$ is the forcing amplitude, $\tilde{T}$ is the fundamental wave period, and j is a chosen number of fundamental wave periods.

A damping layer is employed at the top of the domain as a non-reflecting lid. The damping layer is Rayleigh friction [23], where the quantity $\beta\tilde{\vec{u}}$ is included in the momentum equations. The damping layer is similar as that used by Klemp and Lilly [15], and discussed further by Durran [9]. The damping terms are treated explicitly, and any derivatives of β that arise in the formulation are neglected.

Filtering is used to avoid the accumulation of energy at the highest resolved frequencies. Filtering is achieved here using the sequence of spectral filters discussed by Vandeven [32]. The filter is defined by

$$\omega(\zeta) = 1 - \frac{(2p-1)!}{[(p-1)!]^2}\int_0^\zeta [\xi(1-\xi)]^{p-1} d\xi, \tag{101}$$

where ω is the filter value, ζ is the frequency, ξ is a dummy variable for ζ, and p is the integer order of the filter. This integral may be evaluated analytically to obtain

$$\omega(\zeta) = \sum_{q=1}^{p} \frac{(2p-1)!}{(p-1)!(2p-q)!}\zeta^{q-1}(1-\zeta)^{2p-q}. \tag{102}$$

This family of filters becomes increasingly sharp as p increases, and were proven by Vandeven [32] to retain spectral accuracy. In addition, some of the more common filters can be shown to be members of this sequence. The velocity and potential temperature fields were filtered in all directions at each time step for a fixed value of p. The value of $p = 15$ was generally found to be sufficient. Furthermore, simulations of the linear equations with and without filtering with this value of p demonstrated no significant effects on the basic wave.

All cases reported here use a resolution of 128×128. A number of cases with higher resolution, up to 512×512, have been considered, and show that the results are not significantly changed. Similarly, the time step is set to $\Delta\tilde{t} = 0.1$ for all results, after a substantial effort to demonstrate insensitivity to the time step.

3.4 Results

Results are obtained for two cases; 1) λ of 10 km and 2) λ of 100 km (λ is the horizontal wavelength of the forcing). The parameter values for case 1 and

2 are shown in tables 1 and 2, respectively. Case 1 was chosen as typical of internal waves in the atmosphere, while case 2 proved to be more convenient for studying large amplitude forcing and wave breaking.

Results for case 1 are shown in figures 2, 3, and 4. The profile indicated by the solid line in figure 2 is a vertical slice of vertical velocity, $\tilde{w}$, at three time values. The profile indicated by a dashed line in figure 2 is the same case repeated without nonlinear effects. Note that the horizontal dashed line shows the vertical position of the interface in all figures.

The wave packet that is created by the bottom forcing is chosen to have a vertical length equal to two vertical wavelengths of the fundamental wave, while the distance between the bottom boundary and the interface is approximately 2.7 times this same vertical wavelength. Hence, the wave packet for case 1 'fits' between the bottom boundary and the interface. Figure 2a shows the wave packet is below the interface, but beginning to interact with it. The results in figure 2b are for a later time where the wave packet has already interacted with the interface, creating transmitted and reflected waves, both substantially weaker than the incident waves. In figure 2c, the reflected waves have impacted the bottom of the domain and reflected again, however the packet has now lost much of its coherence.

Figure 3 shows the horizontal average of horizontal velocity, $\langle \tilde{u} \rangle$, for the same times as figure 2. Figure 3a shows that there is a horizontal mean flow aligned with the wave packet. The simulations show that this mean flow moves with the wave packet, as discussed previously by Sutherland [29] using constant N throughout.

A different result is evident in the average horizontal velocity shown in figure 3b and 3c; the wave packet develops a horizontal mean flow, concentrated near the interface. Note that the wave packet in figure 2b at $\tilde{t} = 1000$ has moved beyond the interface, yet the mean flow shown in figure 3b remains. Figure 3c shows that this mean flow at $\tilde{t} = 1500$ is largely unchanged. Much later times, when the wave motion has completely dissipated, show that this mean flow remains permanently.

These results indicate that there are two components to the mean flow, the mean flow that is associated with the wave packet, moving with the packet, and the mean flow at the interface that becomes a permanent feature of the flow, even after the waves are gone. The strength of both components of the mean flow depends strongly on the amplitude of the wave. However, the character of the mean flow does not change dramatically with wave amplitude. For example, figure 5 shows the normalized mean flow for case 1 with

three values of forcing amplitude, $\tilde{\alpha} = 0.01$, 0.05, and 0.1. The normalized mean flow is defined as

$$\frac{\langle \tilde{u} \rangle}{\tilde{\alpha}^2}. \tag{103}$$

Figure 5 shows that this normalized mean flow is nearly identical for the three different amplitudes. This is true for both the packet mean flow, figure 5a, and the interfacial mean flow, figure 5b.

The mean flow is obtained by solving (99), which is the horizontal average of (69). The presence of the interfacial mean flow can be explained as a consequence of the change in momentum flux, $\langle \tilde{\bar{\rho}} \tilde{u} \tilde{w} \rangle$. Integrate (99) across the interface to obtain

$$\frac{\partial}{\partial \tilde{t}} \int_{\tilde{z}} \tilde{\bar{\rho}} \langle \tilde{u} \rangle \, d\tilde{z} = \langle \tilde{\bar{\rho}} \tilde{u} \tilde{w} \rangle \big|_{\text{below}} - \langle \tilde{\bar{\rho}} \tilde{u} \tilde{w} \rangle \big|_{\text{above}}, \tag{104}$$

The momentum flux, $\langle \tilde{\bar{\rho}} \tilde{u} \tilde{w} \rangle$, above the interface is much small than below the interface, due to the wave reflection. The wave reflection is necessary to meet the interfacial conditions, even for linear waves, as discussed in the previous section. The decrease in $\langle \tilde{\bar{\rho}} \tilde{u} \tilde{w} \rangle$ across the interface makes the right-hand-side of (104) positive, which can only be balanced by an increase in $\langle \tilde{u} \rangle$; a horizontal acceleration. More generally, since the side boundary conditions are periodic, and the flow inviscid, then there is no net force to counter the change in momentum caused by the wave reflection. The horizontal acceleration appears instead. Further evidence is provided by the normalized mean velocity, figure 5, which shows that the strength of the mean flow depends approximately on the *square* of the amplitude, as does the momentum flux.

The behavior in the region beneath the interface changes dramatically during the evolution of the wave packet, as can be seen in figure 2. In figure 2a, the wave packet is well-defined, while in figure 2c, the motion is reduced to a standing wave oscillation. This feature is more clearly shown in figure 4 with contours of the vertical velocity at times that correspond to figures 2 and 3. Figure 4a shows the coherent wave packet in the lower layer, while figure 4c shows that the wave packet is now a standing wave, with the vertical wavelength equal to the vertical distance from the bottom to the interface.

Once the standing wave oscillation begins in earnest, the strength decreases as wave energy is transmitted through the interface. The resulting behavior in the upper layer during this period is a temporally decaying mode that is evanescent in the upper layer, meaning that the wave amplitude decreases with increasing altitude. Note that an evanescent mode does not exist if

the waves are allowed to fill the entire domain and become fully-developed, as indicated in the previous section. Evanescent behavior can be seen at earlier times, before the standing oscillation is predominant. For example, the behavior in the upper layer in Figure 2b shows that the transmitted wave has an evanescent profile.

Contours of total potential temperature (not shown), which are often used to indicate wave overturning [33], clearly show that the waves are not overturning for case 1 for the amplitudes mentioned above. Higher amplitude forcing has been found to result in a shear flow instability at the bottom of the domain, as a result of the mean flow created near the wavemaker. This phenomenon makes it difficult to create large amplitude waves for the parameter values of case 1. Hence the results of case 1 correspond to a relatively small amplitude. This can be seen in figure 2, which shows profiles of $\tilde{w}$ for linear (dashed line) as well as nonlinear cases. The difference between linear and nonlinear is largest in figure 2b below the interface, where incident waves and reflected waves are interacting, but overall the differences are not large.

The results for case 2 are shown in figures 6-17 for three forcing amplitudes. Figure 6, 7, and 8 show profiles of vertical velocity, mean horizontal velocity, and contours of vertical velocity, respectively, for three time values and with a forcing amplitude of 0.1 (as for case 1). Figure 9 shows contours of total potential temperature for the same times. The interface is again indicated with the dashed line.

The times for figures 6a and 6b correspond to when the wave packet is interacting with the interface. The vertical position of the wave packet can be seen clearly in the contours of vertical velocity, shown in figure 8. This case (case 2) does not leave behind a strong standing wave, as did case 1. The transmitted wave packet remains coherent and continues to ascend, growing in amplitude. Finally, convective overturning occurs, as can be seen in the contours of total potential temperature shown in figure 9c. The waves 'break' at this point in the simulation. With the chosen filter ($p = 15$), the simulation cannot continue. Stronger filtering would be required.

Note in figure 7c that the mean flow at the interfacial altitude has not changed from the mean flow in figure 7b at an earlier time. The wave packet has moved beyond the interface and left this interfacial mean flow behind, as with the previous case. The strong mean flow above the interface in figure 7c is moving with the wave packet.

The contours of total potential temperature for the earlier times, shown in figure 9a and 9b, show that the wave steepens considerably during the

interaction with the interface. Figure 9b shows in fact that the wave nearly overturns; closer examination shows that it does not. This wave steepening appears to be directly related to the presence of the mean flow, as will be seen.

Results for a higher amplitude, $\tilde{\alpha} = 0.15$, are shown in figures 10-13. The evolution of the wave packet is very similar with this larger amplitude. In particular, figure 11 shows that the interfacial mean flow has the same form as in figure 7, except now is stronger. A significant difference is evident in the contours of total potential temperature, shown in figure 13. Figure 13a shows that the wave is overturning below the interface. Figure 13b indicates that breaking has occurred below the interface, and the filtering has managed to suppress the small scale activity that is created during the breaking event.

The wave packet has moved past the interface in figure 13c, and has reach an amplitude where breaking is occurring again. The position of the wave packet is evident in the profiles of $\tilde{w}$ in figure 10, and contours of $\tilde{w}$ in figure 12. Note that the altitude for breaking is lower than the altitude for breaking in figure 9c for the case with $\tilde{\alpha} = 0.1$.

Results for an even higher amplitude, $\tilde{\alpha} = 0.2$, are shown in figures 14-17. Once again, the only difference is the value of the forcing amplitude; all other parameters are set to the values for case 2 listed in table 2. The wave dynamics are again similar, except now the wave breaks more violently below the interface. This can be seen in the contours of total potential temperature, figure 17. The filtering is not sufficient to control this breaking event, and the smallest scales are overwhelmed. The simulation cannot continue without added filtering.

It can be seen in figures 14-17 that the wave packet has been transmitted, and is developing another breaking event. This is most evident in figure 17b, which shows the contours of total potential temperature as they steepen.

The wave breaking below the interface can be explained as a consequence of the interfacial mean flow. The horizontal phase velocity of a linear wave in this rescaled system, neglecting the inverse of the scale height, is

$$\tilde{c}_p = \tilde{\sigma}, \tag{105}$$

It is well-known that an internal wave attempting to transit a mean shear flow will experience a critical layer at the place where the parallel component of wave speed is equal to the local mean velocity. The forcing frequency, and therefore the horizontal wavespeed, for case 2 is approximately unity. The

interfacial mean flow with $\tilde{\alpha} = 0.1$ has a maximum value of approximately unity, as shown in figure 7b. This mean flow apparently caused the wave steepening shown in figure 9b, but was not strong enough to cause overturning.

The maximum value of the interfacial mean flow with $\tilde{\alpha} = 0.15$ was greater than unity, and greater than the horizontal wave speed. This mean flow is strong enough to overturn the waves, as is evident in figure 13. And finally, with $\tilde{\alpha} = 0.2$, the mean flow is much greater than unity, resulting in a much more violent breaking event.

One final comment concerns the location of breaking. All simulations to date show that the interfacial mean flow causes breaking *below* the interface, never above. In fact, the wave amplitude immediately above the interface is greatly reduced by interfacial reflection or wave breaking. This indicates that wave-induced turbulence in the atmosphere is expected in the region below the tropopause, not above. This is in contrast to the conclusions of Van Zandt and Fritts [31], who argued that wave breaking and turbulence are expected above the tropopause, rather than below.

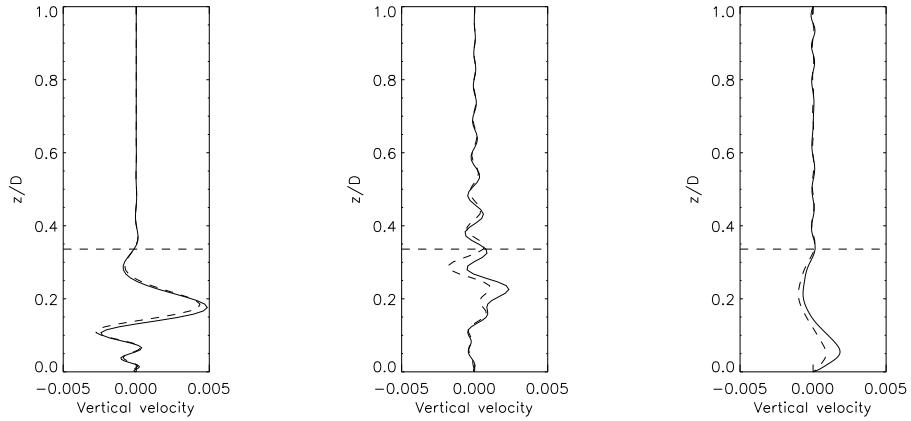

(a) $\tilde{t} = 500$ (b) $\tilde{t} = 1000$ (c) $\tilde{t} = 1500$

Figure 3: Profiles of vertical velocity, $\tilde{w} = \frac{w}{\sqrt{g\lambda}}$, for case 1 with $\tilde{\alpha} = 0.1$ (the dashed profile is linear)

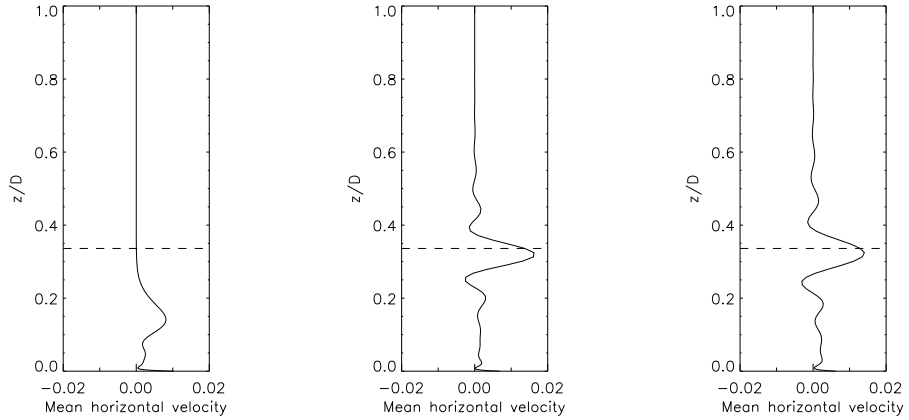

(a) $\tilde{t} = 500$ (b) $\tilde{t} = 1000$ (c) $\tilde{t} = 1500$

Figure 4: Mean horizontal velocity, $\langle \tilde{u} \rangle$, for case 1 with $\tilde{\alpha} = 0.1$

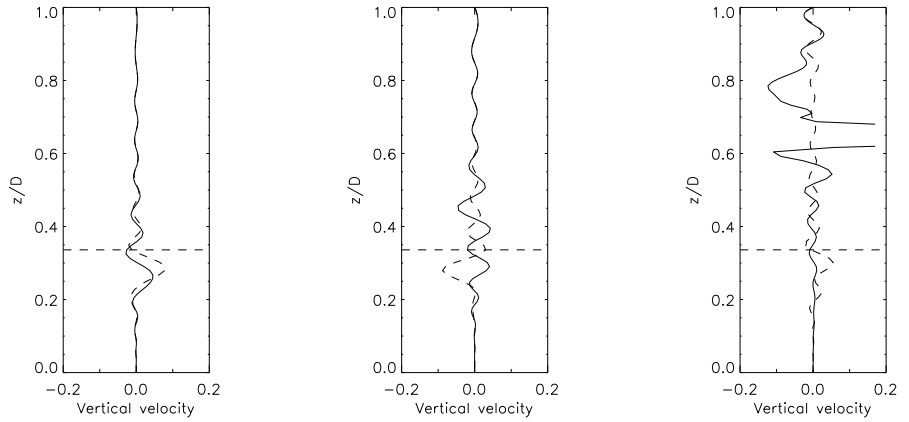

(a) $\tilde{t} = 240$ (b) $\tilde{t} = 270$ (c) $\tilde{t} = 340$

Figure 5: Profiles of vertical velocity, $\tilde{w} = \frac{w}{\sqrt{g\lambda}}$, for case 2 with $\tilde{\alpha} = 0.1$ (dashed profile is linear)

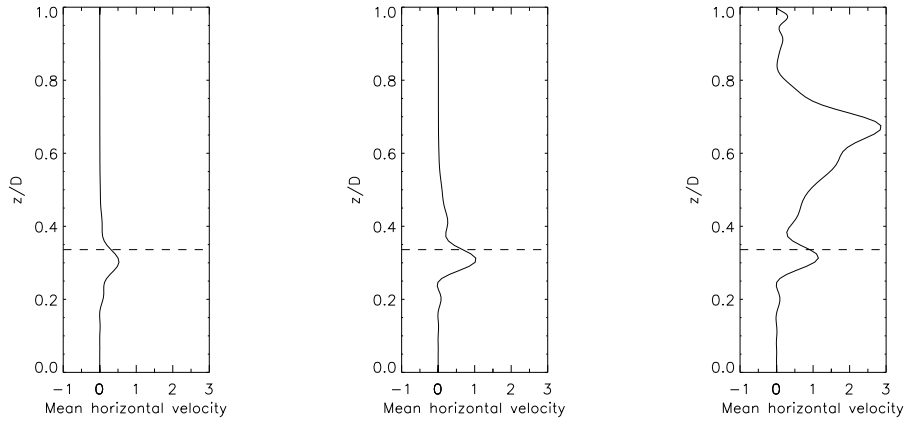

(a) $\tilde{t} = 240$ (b) $\tilde{t} = 270$ (c) $\tilde{t} = 340$

Figure 6: Mean horizontal velocity, $\langle \tilde{u} \rangle$, for case 2 with $\tilde{\alpha} = 0.1$

4 Non-Boussinesq internal waves

Internal waves in a non-Boussinesq atmosphere have an exponentially growing amplitude, becoming unbounded in an unbounded domain. Weakly nonlinear non-Boussinesq theory must contend with this unbounded linear behavior, and result in higher harmonics that grow exponentially with an even faster rate. This problem is an impediment to further theory of non-Boussinesq waves. An alternative expansion has been found, and has been published in SIAM Journal of Applied Math [3].

Internal waves of permanent form are horizontally periodic waves where the wave amplitude does not evolve. Weakly nonlinear theory of internal waves of permanent form in a continuously stratified fluid was previously considered by Thorpe [30] and Yih [36], both treating incompressible inviscid flow between two rigid horizontal surfaces assuming constant Brunt-Vaisala frequency. Thorpe [30] showed that the waves generate a mean flow, but he did not determine a nonlinear contribution to the wave speed. Yih [36] determined the wave-induced mean flow by adjusting the background state, and found a second-order correction to the wavespeed.

Yih's results are surprising, and show that the second-order wavespeed correction is negative. A negative value means that larger amplitude waves travel slower than small amplitude waves, opposite the case for most wave systems, such as free surface waves. Yih only reported results with a horizontal wave-number of unity.

Both Thorpe and Yih used a straight-forward expansion in the wave amplitude; for example, Yih [36] expanded the streamfunction, ψ, using

$$\psi = \psi_0 + \epsilon\psi_1 + \epsilon^2\psi_2 + \cdots \tag{106}$$

where $\epsilon << 1$ is the wave amplitude. The linear solution has the form

$$\psi_1 = e^{\frac{\beta}{2}z} \sin kx \sin mz, \tag{107}$$

where k and m are the horizontal and vertical wavenumbers, respectively, and β is the Boussinesq parameter. The product of the constant wave amplitude and the exponential growth, $\epsilon e^{\frac{\beta}{2}z}$, is often thought of as an exponentially growing wave amplitude. This characteristic is well-known in atmospheric waves [13], and all non-Boussinesq internal waves.

[3] J. McHugh, SIAM Journal of Applied Math, **66**, pp. 1845-1855, 2009.

The second-order solution must contend with nonlinear quadratic terms, and Yih's resulting expression for ψ_2 contains a term similar to

$$\psi_2 = \cdots \epsilon^2 e^{\beta z} \sin 2kx \sin 2mz \cdots , \tag{108}$$

along with many other terms. Note that the exponential growth with altitude of ψ_2 is twice the exponential growth of ψ_1. The third order equation contains cubic terms, resulting in the behavior $e^{\frac{3\beta}{2}z}$, and finally the n^{th} order solution would contain $e^{\frac{n\beta}{2}z}$ behavior. Clearly the rate of growth is increasing with each term. This straight-forward expansion in wave amplitude does not converge at any altitude, but is asymptotic if the top boundary is a rigid lid. If different top boundaries are treated, the results with this expansion are not valid.

An alternative expansion that is more generally valid is considered here. The new expansion is suggested by the following 'model' equation, obtained by arbitrarily discarding terms from the governing equation:

$$u_z - u + u^2 = 0, \tag{109}$$

where $u = u(z)$. The exact solution is readily obtained:

$$u = \frac{\epsilon e^z}{1 + \epsilon e^z}, \tag{110}$$

where ϵ is a constant.

Let $\zeta = \epsilon e^z$ for convenience, and the exact solution becomes

$$u = \frac{\zeta}{1 + \zeta}. \tag{111}$$

Note the singular point at $\zeta = -1$. A McLauren series expansion of (111) is

$$u = \sum_{n=1}^{\infty} \big(-1 \big)^n \zeta^n = \epsilon e^z - \epsilon^2 e^{2z} + \epsilon^3 e^{3z} + \cdots . \tag{112}$$

The presence of the singular point limits the validity of (112) to $\zeta < 1$. This McLauren expansion is analogous to the expansion used by both Thorpe [30] and Yih [36].

An expansion without this limitation is a Laurent expansion about $\zeta = -1$ of the form

$$u = \sum_{n=0}^{\infty} a_n \left[\frac{1}{\zeta + 1} \right]^n . \tag{113}$$

The coefficients can be found by merely rearranging the exact solution:

$$u = \frac{\zeta}{1+\zeta} = 1 - \frac{1}{1+\zeta}, \tag{114}$$

resulting in $a_0 = 1$, $a_1 = -1$, and $a_n = 0$ for $n > 1$. Hence the exact solution to the model equation is equivalent to this Laurent expansion about $\zeta = -1$. The results of this model equation suggest that a Laurent-type expansion may provide a solution that is more generally valid, and such a solution is considered here. The dependent variable will be expanded in a series of the form

$$\sum_{p=1}^{\infty} \left(\frac{\epsilon e^{\alpha z}}{1 + \epsilon e^{\alpha z}} \right)^p \phi_p\big(x, z\big), \tag{115}$$

where α is a constant yet to be determined, and p is an integer. For the nonlinear case, only the first few terms of this expansion can be determined, due to the complexity of the equations. For this reason, the results are only valid for small amplitude, as with Yih's previous theory.

The results found with the new expansion show that the second-order correction is positive or negative, depending on wave parameters. Furthermore, the wave amplitude with this new expansion no longer shows an unbounded exponential growth with altitude. Instead the wave amplitude experiences an exponential growth with altitude, but then asymptotically approaches a constant value. This behavior of wave amplitude is often called saturation [11, 25, 26], and waves whose amplitude no longer grows with altitude are saturated waves. The results with the new expansion show the same general trends as Yih's original expansion.

This new result is discussed below in section 5. Section 2 discusses the equations governing the problem, section 3 gives the linear solution, showing that it is identical to the well-known linear solution, and section 4 gives some of the details of the weakly nonlinear analysis.

4.1 Basic equations and Long's equation

The flow is assumed to be incompressible, inviscid, and two-dimensional, governed by the Euler equations, the continuity equation, and the equation of incompressibility:

$$\rho \frac{Du}{Dt} = -\frac{\partial p}{\partial x}, \tag{116}$$

$$\rho \frac{Dw}{Dt} = -\frac{\partial p}{\partial z} - \rho g, \tag{117}$$

$$\frac{\partial u}{\partial x} + \frac{\partial w}{\partial z} = 0, \tag{118}$$

$$\frac{D\rho}{Dt} = 0, \tag{119}$$

where (u, w) are the velocities in the (x, z) directions, respectively, p is the pressure, ρ is the density, and g is the gravitational constant.

If a coordinate system is chosen to move with the waves, then the flow is steady, and Longs equation (3) may be used. The system is made dimensionless using a velocity scale, U, to be defined later, a constant value of density, ρ_{00}, and the layer thickness, d:

$$\hat{\delta} = \frac{\delta}{d},\ \hat{x} = \frac{x}{d},\ \hat{z} = \frac{z}{d},\ \hat{\rho} = \frac{\rho}{\rho_{00}}. \tag{120}$$

Dropping the circumflex, Long's equation becomes

$$\nabla^2 \delta + \frac{1}{2}\frac{1}{q}\frac{dq}{dz_0}\left[2\frac{\partial \delta}{\partial z} - \big(\nabla \delta\big)^2\right] + \frac{\beta}{F_r^2 u_0^2}\delta = 0, \tag{121}$$

where

$$F_r = \frac{U}{\sqrt{gd}}, \tag{122}$$

is the Froude number.

4.2 Linear solution

Equation (3) requires the flow to be steady. Steady flow with traveling waves is achieved by choosing the coordinate system to be moving with the horizontal wavespeed, c. This approach is adopted for the linear case by choosing $F_r u_0 = c$. Note that the nonlinear theory will include a wave-induced mean flow, and u_0 must account for part of this, as will be seen.

Linearize Long's equation to obtain

$$\nabla^2 \delta - \beta \delta_z + \frac{\beta}{c^2}\delta = 0. \tag{123}$$

Expand δ with

$$\sum_{p=1}^{\infty} \left(\frac{\epsilon e^{\alpha z}}{1 + \epsilon e^{\alpha z}}\right)^p \phi_p\big(x, z\big), \tag{124}$$

where ϕ_p are yet to be determined. Insert (124) into (123), and collect on powers of the quantity $\frac{\epsilon e^{\alpha z}}{1+\epsilon e^{\alpha z}}$. A successful choice for α is

$$\frac{\beta}{2}. \tag{125}$$

The resulting coefficient of $\left(\frac{\epsilon e^{\alpha z}}{1+\epsilon e^{\alpha z}}\right)^p$ is

$$\begin{aligned}\nabla^2\phi_p + \big(p-1\big)\beta\phi_{p_z} + \left[\frac{\beta}{c^2} + p\big(p-2\big)\frac{\beta^2}{4}\right]\phi_p = \\ \big(p-1\big)\beta\phi_{p-1_z} + \big(p-1\big)\big(2p-3\big)\frac{\beta^2}{4}\phi_{p-1} \\ -\big(p-1\big)\big(p-2\big)\frac{\beta^2}{4}\phi_{p-2}.\end{aligned} \tag{126}$$

for all $p \geq 1$.

A solution for all p is

$$\phi_p = \sin kx \sin mz, \tag{127}$$

where k and m are constants. Equation (126) at each order results in

$$c^2 = \frac{\beta}{k^2 + m^2 + \frac{\beta^2}{4}}, \tag{128}$$

the familiar dispersion relation.

The final result is

$$\delta = \left[\sum_{p=1}^{\infty}\left(\frac{\epsilon e^{\frac{\beta}{2}z}}{1+\epsilon e^{\frac{\beta}{2}z}}\right)^p\right]\sin kx \sin mz, \tag{129}$$

where $\cos mz$ may be substituted for $\sin mz$. This solution may be verified by direct substitution.

Each $p > 1$ could also include a homogeneous solution, with two arbitrary constants. These homogeneous solutions have the form

$$\phi_p = e^{-\frac{p-1}{2}\beta z}\sin kx \sin mz. \tag{130}$$

Note that these homogeneous solutions beyond $p = 1$ have exponential *decay* with altitude, hence these homogeneous components do not compromise the uniform validity of the result of the next section.

The solution in (129) is identical to the traditional linear solution with an exponential growing wave amplitude, as can be demonstrating by quoting the well know expansion,

$$e^{\alpha} = \sum_{p=1}^{\infty} \left(\frac{e^{\alpha}}{1+e^{\alpha}} \right)^{p}. \tag{131}$$

4.3 Weakly nonlinear waves with rigid boundaries

A continuously stratified layer of fluid with rigid top and bottom will now be treated with the expansion of the previous section. This is the same problem treated by Yih [36] and Thorpe [30].

The governing equation is (3). Define Q:

$$Q = \frac{\epsilon e^{\alpha z}}{1+\epsilon e^{\alpha z}}. \tag{132}$$

Expand δ in a power series:

$$\delta = Q\phi_1 + Q^2\phi_2 + \cdots, \tag{133}$$

where ϕ_j are not the same as the linear solution. Note that the analysis is aided by the relation

$$\frac{d}{dz}(Q)^p = \alpha p \Big[(Q)^p - (Q)^{p+1} \Big]. \tag{134}$$

Two features are anticipated; 1) the waves will create a mean flow at second order, and 2) the wavespeed must be adjusted at second order to obtain a uniformly valid solution. In the linear theory of the previous section, the upstream velocity, u_0, was chosen to be the constant wavespeed, c, making the waves of permanent form steady. For the present nonlinear theory, a coordinate system is again chosen to move with the waves, however choosing u_0 to be constant does not provide a success result. Instead, the wavespeed and part of the wave-generated mean flow are merged together as u_0, and then this is expanded in the same manner:

$$F_r u_0 = c_0 \Big[1 + Qc_1 + Q^2 c_2 + \cdots \Big], \tag{135}$$

where the c_j's are constants. The constant, c_0, will be equal to the linear wavespeed, and the remaining c_j's will be chosen to obtain a uniformly valid solution.

The work of Yih shows that the upstream density profile must be adjusted so the the density profile *in the presence of waves* results in the desired profile. This correction is included at this early stage by expanding β:

$$\beta = \beta_0 \Big[1 + Q\beta_1 + Q^2\beta_2 + \cdots \Big], \tag{136}$$

where the β_j's also constants.

4.3.1 First order

Insert (133), (135), and (136) into (3) and collect the coefficient of Q to obtain

$$\nabla^2\phi_1 + \Big[2\alpha - \beta_0 \Big] \phi_{1z} + \left[\frac{\beta_0}{c_0^2} - \beta_0\alpha + \alpha^2 \right] \phi_1 = 0. \tag{137}$$

If

$$\alpha = \frac{\beta_0}{2}, \tag{138}$$

matching the value of the linear solution, then (137) becomes

$$\nabla^2\phi_1 + \left[\frac{\beta_0}{c_0^2} - \frac{\beta_0^2}{4} \right] \phi_1 = 0. \tag{139}$$

The solution to (139) is

$$\phi_1 = \sin kx \sin mz, \tag{140}$$

where k is constant,

$$m = n\pi \tag{141}$$

for any integer, n, and (128) determines c_0. Note that (139) along with (141) satisfies the boundary conditions at $z = 0, 1$.

4.3.2 Second order

Using the choice for α given by (138), the second-order equation is

$$\begin{aligned}\nabla^2\phi_2 + \beta_0\phi_{2z} + \frac{\beta_0}{c_0^2}\phi_2 = \quad & \beta_0\phi_{1z} + \frac{\beta_0^2}{4}\phi_1 \\ & -\frac{1}{2}\beta_0\left[{\phi_1}_x^2 + \left(\phi_{1z} + \frac{\beta_0}{2}\phi_1\right)^2\right] \\ & -c_1\left[\beta_0\phi_{1z} + \frac{\beta_0^2}{2}\phi_1 - 2\frac{\beta_0}{c_0^2}\phi_1\right] \\ & +\beta_1\left[\beta_0\phi_{1z} + \frac{\beta_0^2}{2}\phi_1 - \frac{\beta_0}{c_0^2}\phi_1\right].\end{aligned} \tag{142}$$

Note that the first two terms on the right-hand-side are part of the linear solution.

The value for β_1 is chosen to match the upstream conditions, and has been found to be zero, in agreement with the results of Yih [36]. Details of this correction are delayed until later, when the correction is not zero. The value of c_1 is chosen to assure a uniformly valid solution, and has also been found to be zero, in agreement with both Thorpe [30] and Yih [36].

A homogeneous solution to (142) must be included in order to meet the boundary conditions. The necessary solutions are

$$e^{-\frac{\beta_0}{2}z}\left[a\cos\mu z + b\sin\mu z\right], \tag{143}$$

and

$$e^{-\frac{\beta_0}{2}z}\left[a\cos\gamma z + b\sin\gamma z\right]\sin 2kx. \tag{144}$$

where

$$\mu^2 = G_0 - \frac{\beta_0^2}{4}, \tag{145}$$

$$\gamma^2 = G_0 - 4k^2 - \frac{\beta_0^2}{4}. \tag{146}$$

If $\gamma^2 < 0$ or $\mu^2 < 0$, then a hyperbolic form is chosen for (143) or (144), respectively.

The final expression for ϕ_2 is

$$
\begin{aligned}
\phi_2 = &\sin kx \sin mz \\
&+ \beta_0 \Bigg\{ \frac{B_1}{G_0} \Bigg[\Bigg(\cos \mu z + \big(e^{\frac{\beta_0}{2}} - \cos \mu\big) \frac{\sin \mu z}{\sin \mu} \Bigg) e^{-\frac{\beta_0}{2} z} - 1 \Bigg] \\
&+ \frac{D_1}{G_0 - 4m^2} \Bigg[\Bigg(\cos \gamma z + \big(e^{\frac{\beta_0}{2}} - \cos \gamma\big) \frac{\sin \gamma z}{\sin \gamma} \Bigg) e^{-\frac{\beta_0}{2} z} - 1 \Bigg] \cos 2kx \\
&+ \frac{B_2\big(G_0 - 4m^2\big) + B_3\big(2m\beta_0\big)}{M} \Bigg[\Bigg(\cos \mu z + \big(\cos 2me^{\frac{\beta_0}{2}} - \cos \mu\big) \frac{\sin \mu z}{\sin \mu} \Bigg) e^{-\frac{\beta_0}{2} z} \\
&\qquad\qquad - \cos 2mz \Bigg] \\
&- \frac{B_2\big(2m\beta_0\big) + B_3\big(G_0 - 4m^2\big)}{M} \sin 2mz \\
&- \frac{D_2 P - B_3\big(2m\beta_0\big)}{N} \Bigg[\Bigg(\cos \gamma z + \big(\cos 2me^{\frac{\beta_0}{2}} - \cos \gamma\big) \frac{\sin \gamma z}{\sin \gamma} \Bigg) e^{-\frac{\beta_0}{2} z} \\
&\qquad\qquad - \cos 2mz \Bigg] \cos 2kx \\
&+ \frac{D_2\big(2m\beta_0\big) - B_3 P}{N} \sin 2mz \cos 2kx \Bigg\}.
\end{aligned}
$$

where G_0, B_1, B_2, B_3, M, P, and N are given in Appendix I, and are defined as in Yih [36] to allow for direct comparison.

4.3.3 Third order

The third-order equation is

$$
\begin{aligned}
\nabla^2 \phi_3 + 2\beta_0 \phi_{3z} + \left[\frac{\beta_0}{c_0^2} + 3\frac{\beta_0^2}{4} \right] \phi_3 = &\, 2\beta_0 \phi_{2z} + 6\frac{\beta_0^2}{4} \phi_2 - \frac{\beta_0^2}{2} \phi_1 \qquad (147) \\
&-\beta_0 \left[\phi_{1x} \phi_{2x} + \left(\phi_{1z} + \frac{\beta_0}{2} \phi_1 \right) \left(\phi_{2z} + \frac{\beta_0}{2} \phi_2 - \frac{\beta_0}{2} \phi_1 \right) \right] \\
&-2c_2 \left[\beta_0 \phi_{1z} + \frac{\beta_0^2}{2} \phi_1 - \frac{\beta_0}{c_0^2} \phi_1 \right] \\
&+\beta_2 \left[\beta_0 \phi_{1z} + \frac{\beta_0^2}{2} \phi_1 - \frac{\beta_0}{c_0^2} \phi_1 \right],
\end{aligned}
$$

This equation will be used to determine c_2; no attempt will be made to determine ϕ_3 in its entirety.

Before finding c_2, it is necessary to determine β_2 so that the upstream density profile matches the density profile in the presence of waves averaged over one wavelength. Following Yih [36], the definition of δ in (4) and the above solution to second order are used to obtain

$$z = z_0 + Q\phi_1 + Q^2\phi_2. \tag{148}$$

This is a nonlinear algebraic equation for the shape of a streamline, $z = \eta(x, z_0)$, for a chosen value of z_0. A streamline in this scenario is also a line of constant density, and the relationship between ρ and z upstream could be used to eliminate z_0, resulting in $z = \eta(x, \rho)$. The inversion of this relationship is the density in the disturbed field, $\rho(x, z)$.

Equation (148) is inverted using the method of successive approximations, as in Stokes [28] and Yih [36], and then averaged over a wavelength to obtain

$$\overline{\eta} = z_0 + \left[\frac{\epsilon e^{\frac{\beta_0}{2}z_0}}{1 + \epsilon e^{\frac{\beta_0}{2}z_0}}\right]^2 \Bigg\{ \Big(h_1 + h_3\Big) e^{-\frac{\beta_0}{2}z_0} \cos \mu z_0$$
$$+ \Big(h_1 + h_3\Big) F_3(\mu) e^{-\frac{\beta_0}{2}z_0} \sin \mu z_0 - h_3 \cos 2mz_0 - h_4 \sin 2mz_0 - h_1 \Bigg\}, \tag{149}$$

where expressions for the h_j and F_3 are provided in Appendix II.

The correction is now found using the approach of Yih:

$$\frac{1}{\rho_0}\frac{d\rho_0}{dz_0} = \frac{1}{\rho}\frac{d\rho}{d\overline{\eta}}\frac{d\overline{\eta}}{dz_0} = -\beta_0 \frac{d\overline{\eta}}{dz_0}, \tag{150}$$

which may be further evaluated by taking a derivative of (149). The effect is only felt at second order, and is accounted for by choosing β_2:

$$\beta_2 = \beta_0 \Bigg\{ \left[\Big(\mu F_3(\mu) + \frac{\beta_0}{2}\Big) \cos \mu z + \Big(\frac{\beta_0}{2} F_3(\mu) - \mu\Big) \sin \mu z \right] \Big(h_1 + h_3\Big) e^{-\frac{\beta_0}{2}z}$$
$$- \Big(\beta_0 h_3 + 2m h_4\Big) \cos 2mz + \Big(2m h_3 - \beta_0 h_4\Big) \sin 2mz - \beta_0 h_1 \Bigg\}. \tag{151}$$

The last stage of the second-order solution is to determine c_2, found by expanding the right-hand-side of (147) and suppressing secular terms. Equation (147) is multiplied by $e^{\beta_0 z} \sin mz$ and integrated over the vertical domain.

The integral of all terms involving ϕ_3 is exactly zero, as can be demonstrated using Green's second identity and integration-by-parts, making $e^{\beta_0 z}\sin mz$ the correct factor. The final result is

$$c_2 = \frac{1}{8}\beta_0\left[\frac{T_2 + 4T_3 - \beta_0 T_1}{T_4}\right], \tag{152}$$

where T_1, T_2, T_3, and T_4 are provided in appendices. Note that T_1 results from the nonlinear terms in (147), T_2 from the terms involving β_2, T_3 from the $2\beta_0\phi_{2z} + 6\frac{\beta_0^2}{4}\phi_2 - \frac{\beta_0^2}{2}\phi_1$ in (147), and T_4 from the terms involving c_2.

4.4 Results

The complicated expression for c_2 given by (152) has been evaluated numerically for a wide variety of parameters. Results for two modes, $n = 1, 2$, are shown in figures 4.4 and 4.4 using a solid line with $\beta_0 = 0.1$. Note that the dimensionless value of β_0 for atmospheric flows is typically between 0.01 and 0.1, while flows in geophysical bodies of water may have a wider variety of values.

Figure 4.4 shows that for $k \approx 1$, c_2 is negative. This agrees with the previous results of Yih [36], who only reports results for k near unity. For larger k, figure 4.4 shows that c_2 is positive. Figure 4.4 shows that c_2 for the second mode, $n = 2$, is positive, except for very long waves. The physical consequence of a positive c_2 is that higher amplitude internal waves travel faster, often called 'amplitude dispersion'. Amplitude dispersion exists in many other waves systems, in particular, free-surface waves. Amplitude dispersion is important for the existence of certain types of solitary waves. Previous studies of solitary waves in a continuously stratified flow between horizontal walls was considered by Benjamin [5]. Benjamin [5] demonstrated that solitary waves exist for this configuration, but he *assumed* the existence of amplitude dispersion (pointed out by Yih [36]). It was Yih's work showing a negative c_2 that was thought to eliminate this possibility. However, the present results indicate that amplitude dispersion does exist, and solitary waves may form in this configuration. Solitary waves can form in stratified flow under other conditions, as reviewed recently by Pelinovsky, et. al. [22].

A direct comparison with the straight-forward amplitude expansion of Yih may be obtained by expanding Q, as defined in (6), using

$$Q = \epsilon e^{\alpha z} - \epsilon^2\Big(e^{\alpha z}\Big)^2 \cdots \tag{153}$$

and deleting all but the first term. The expansion in Q is then identical to that of Yih, and the present results reduce to exactly the formula's of Yih. The value of c_2 for Yih's expansion are obtained from (152) by deleting the quantity, T_3. The results without T_3 are also plotted in figures 4.4 and 4.4 with a dashed line, and show the same trends as the present results. For all cases considered, the present results predict a wave-speed correction that is greater than that predicted by Yih's expansion.

Figures 4.4 and 4.4 show that c_2 becomes unbounded for isolated values of k. These values correspond to $\gamma = \pm n\pi$, where γ is defined in (146) as part of the second-order homogeneous solution. Hence this singularity appears when the homogeneous solution results in a vertical wavenumber that fits perfectly between boundaries. Yih [36] also found this difficulty, and reports that this singularity will not appear if the analysis is extended to the next order, something that is very difficult to achieve, and is not pursued here. At this time, the value of c_2 near $\gamma = \pm n\pi$ is unclear.

The internal waves discussed here generate a mean flow, as is well-known. This mean flow can be obtained by assembling an expression for δ using (133) and the final result for ϕ_2, then averaging over a horizontal wavelength to obtain $\overline{\delta}$. The final mean flow is obtained when u_0 is combined with the vertical derivative of $\overline{\delta}$. The influence of this wave-induced mean flow on c_2 is measured by the quantity T_2 in (152), and accounts for most of c_2. This was also the case for Yih [36]. Physically, this means that displacement of streamlines is the predominant nonlinear effect, rather than an interaction of higher harmonics.

Note that there is some ambiguity between the wavespeed and the wave-induced mean flow. The initial steps of the analysis chose a coordinate system moving with the nominal wavespeed so that the flow is steady. Any other choice of coordinate system results in an unsteady velocity field. The absolute speed of the waves can only be defined relative to the walls. However, as the boundaries have no shape, and the horizontal velocity of the boundaries is irrelevant in inviscid flow, there is no method of determining the absolute wavespeed. The second-order correction to c_0 is given by $Q^2 c_2$. Since Q^2 is positive definite, then the sign of this correction is determined by the sign of c_2. Furthermore, Q contains the small parameter, ϵ, and cannot be larger than the linear wavespeed. This means that the wave-speed correction causes the wave pattern to move faster or slower, depending only on the wave amplitude and the sign of c_2. This feature still represents amplitude dispersion, despite this ambiguity.

A vertical slice of δ at second order for an example set of parameters shows that this wave envelope is a second-order saturated wave.

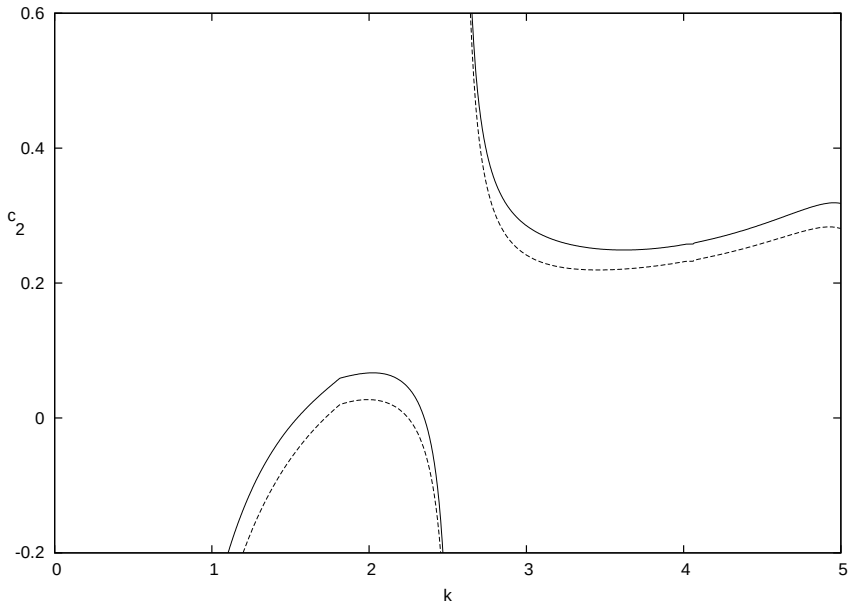

Figure 7: Second-order correction to the wavespeed with $n = 1$ and $\beta_0 = 0.1$

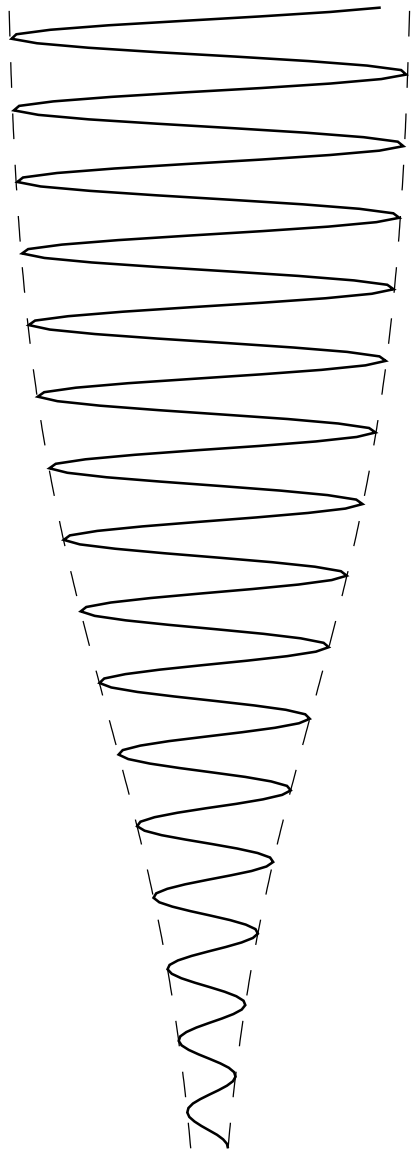

Figure 8: Second-order envelope shape

5 Nonlinear Schrödinger equations for a wave packet at the interface

Consider two layers, with each layer distinguished by the value of the Brunt-Vaisala frequency, assumed constant within each layer. The density profile is continuous at the interface. The flow is modeled with the Boussinesq approximation.

A packet of internal waves approach the interface between the two layers from below. The waves are horizontally periodic. The weakly nonlinear theory is considered below.

5.1 Governing equations

Assume incompressible flow, and neglect any diffusion. The flow is assumed to be incompressible, inviscid, and two-dimensional. Stratification is present due to the presence of a non-diffusing quantity, and the flow is assumed to be Boussinesq. The flow is then governed by the Euler equations in Boussineq form, the continuity equation, and the equation of incompressibility:

$$\rho_0 \frac{Du}{Dt} = -\frac{\partial \hat{p}}{\partial x}, \tag{154}$$

$$\rho_0 \frac{Dw}{Dt} = -\frac{\partial \hat{p}}{\partial z} - \hat{\rho} g, \tag{155}$$

$$\frac{\partial u}{\partial x} + \frac{\partial w}{\partial z} = 0, \tag{156}$$

$$\frac{D\hat{\rho}}{Dt} + \frac{d\overline{\rho}}{dz} w = 0. \tag{157}$$

where (u, w) are the velocities in the (x, z) directions, respectively, $\hat{p}$ is the dynamic pressure, ρ_0 is an average (constant) density, $\overline{\rho}(z)$ is the mean density, $\hat{\rho}$ is the density perturbation, and g is the gravitational constant.

It is convenient to put the governing equations in a more convenient form by eliminating all variables in the linear terms in favor of w. The result is

$$\frac{\partial^2}{\partial t^2}\left[\nabla^2 w\right] + N^2 \frac{\partial^2 w}{\partial x^2} = \frac{\partial}{\partial t}\left[\frac{\partial^2 A_1}{\partial x \partial z} - \frac{\partial^2 A_3}{\partial x^2}\right] + \frac{g}{\rho_0}\frac{\partial^2 A_4}{\partial x^2}, \tag{158}$$

where

$$A_1 = u u_x + w u_z, \tag{159}$$

$$A_3 = uw_x + ww_z, \tag{160}$$

$$A_4 = u\hat{\rho}_x + w\hat{\rho}_z, \tag{161}$$

5.2 Interfacial conditions

The mean density profile is chosen to be continuous, but have a discontinous first derivative, such that the fluid exists in two semi-infinite layers, each layer having a unique value of the Brunt-Vaisala frequency. The interface between the two layers must satisfy interfacial conditions. There are two types of interfacial conditions on a material line separating two inviscid layers of fluid; kinematic and dynamic. The kinematic condition in an inviscid flow states that the normal velocity of the material line is equal to the normal component of velocity of the fluid. The dynamic condition states that the pressure must be continuous across the material line.

The kinematic conditions are

$$\eta_t + u^-\eta_x = w^-, \tag{162}$$

$$\eta_t + u^+\eta_x = w^+, \tag{163}$$

which hold on the interface, $z = \eta$, where u^-, w^- are velocities in the lower layer, u^+, w^+ are velocities in the upper layer, and η is the vertical displacement of the interface.

A primary difficulty is meeting the interfacial conditions on the actual interface, $z = \eta$, without knowing the position of the interface beforehand. This difficulty is treated by expanding all terms in a Taylor series about the mean position of the interface, in the same manner usually used for free surface flow. The kinematic conditions become

$$\eta_t + \left[u^- + u_z^-\eta + \frac{1}{2}u_{zz}^-\eta^2 + ...\right]\eta_x = \left[w^- + w_z^-\eta + \frac{1}{2}w_{zz}^-\eta^2 + ...\right], \tag{164}$$

$$\eta_t + \left[u^+ + u_z^+\eta + \frac{1}{2}u_{zz}^+\eta^2 + ...\right]\eta_x = \left[w^+ + w_z^+\eta + \frac{1}{2}w_{zz}^+\eta^2 + ...\right], \tag{165}$$

where the coefficients are now evaluated at the mean position of the interface, $z = 0$.

The dynamic condition is continuity of total pressure, p. Hence

$$p^- = p^+ \tag{166}$$

on $z = \eta$, where p^- and p^+ are the pressures in the lower and upper layers, respectively. Consider the incompressible flow model for now, rather than the more restrictive Boussinesq approximation. The total pressure is segmented into the mean and fluctuating parts:

$$p = \tilde{p} + \hat{p}. \tag{167}$$

Expanding (166) in a Taylor series, as before, gives

$$\begin{aligned}\left[\tilde{p}^- + \hat{p}^-\right]\Big|_{z=0} + \frac{\partial}{\partial z}\left[\tilde{p}^- + \hat{p}^-\right]\Big|_{z=0}\eta + \frac{1}{2}\frac{\partial^2}{\partial z^2}\left[\tilde{p}^- + \hat{p}^-\right]\Big|_{z=0}\eta^2 + \cdots = \\ \left[\tilde{p}^+ + \hat{p}^+\right]\Big|_{z=0} + \frac{\partial}{\partial z}\left[\tilde{p}^+ + \hat{p}^+\right]\Big|_{z=0}\eta + \frac{1}{2}\frac{\partial^2}{\partial z^2}\left[\tilde{p}^+ + \hat{p}^+\right]\Big|_{z=0}\eta^2 + \cdots\end{aligned} \tag{168}$$

Several terms may be eliminated immediately. Pressure in the absence of motion is continuous, which gives $\tilde{p}^- = \tilde{p}^+$ at $z = 0$, allowing these terms to be dropped.

Further simplification is obtained using hydrostatic equilibrium,

$$\frac{\partial \tilde{p}^-}{\partial z} = -\tilde{\rho}^- g, \tag{169}$$

$$\frac{\partial \tilde{p}^+}{\partial z} = -\tilde{\rho}^+ g, \tag{170}$$

where $\tilde{\rho}^-$ and $\tilde{\rho}^+$ are the mean densities in the two layers. The density profile is assumed continuous at the tropopause (although not smooth), implying $\tilde{\rho}^- = \tilde{\rho}^+$ at $z = 0$. Equations (169) and (170) then result in

$$\frac{\partial \tilde{p}^-}{\partial z} = \frac{\partial \tilde{p}^+}{\partial z} \tag{171}$$

on $z = 0$. These two terms may be dropped from (168).

Furthermore, the second derivative of $\tilde{p}$ is related to the Brunt-Vaisala frequency:

$$\tilde{p}_{zz} = -\tilde{\rho}_z g = -\tilde{\rho}\left[g\frac{\tilde{\rho}_z}{\tilde{\rho}}\right] = +\tilde{\rho}N^2, \tag{172}$$

which holds for each layer. Higher order terms result can be treated in a similar manner. The dynamic interfacial condition may now be written as

$$\left[\hat{p}^- - \hat{p}^+\right]_{z=0} + \left[\hat{p}_z^- - \hat{p}_z^+\right]_{z=0}\eta + \frac{1}{2}\left[\hat{p}_{zz}^- - \hat{p}_{zz}^+\right]_{z=0}\eta^2 + \cdots$$
$$+ \frac{1}{2}\tilde{\rho}_0\left[N^{-2} - N^{+2}\right]\eta^2 + \frac{1}{3!}\frac{\tilde{\rho}_0}{g}\left[N^{-4} - N^{+4}\right]\eta^3 + \cdots = 0, \quad (173)$$

where $\tilde{\rho}_0$ is mean density at the interface.

The restriction to Boussinesq flow merely implies that $\tilde{\rho}$ is now taken as the constant, ρ_0.

5.3 Weakly nonlinear theory

Define the following variables:

$$\xi = x - c_p t, \quad (174)$$
$$\zeta = \epsilon z, \quad (175)$$
$$\tau = \epsilon t, \quad (176)$$

where c_p is a constant to be determined later, and ϵ is a small parameter that measures the vertical length of the wave envelope. Assume all variables depend now on ξ, ζ, τ, and z.

The governing equations for each layer become

$$\rho_0\left[(u - c_p)\,u_\xi + \epsilon u_\tau + w u_z + \epsilon w u_\zeta\right] = -\hat{p}_\xi, \quad (177)$$

$$\rho_0\left[(u - c_p)\,w_\xi + \epsilon w_\tau + w w_z + \epsilon w w_\zeta\right] = -\left[\hat{p}_z + \epsilon\hat{p}_\zeta\right] - \hat{\rho}g, \quad (178)$$

$$u_\xi + w_z + \epsilon w_\zeta = 0, \quad (179)$$

$$(u - c_p)\,\hat{\rho}_\xi + \epsilon\hat{\rho}_\tau + w\hat{\rho}_z + \epsilon w\hat{\rho}_\zeta + \tilde{\rho}_z w = 0, \quad (180)$$

These may be rearranged into

$$-\rho_0 c_p u_\xi + \epsilon\rho_0 u_\tau + \hat{p}_\xi = -\rho_0 F_H, \quad (181)$$

$$-\rho_0 c_p w_\xi + \epsilon\rho_0 w_\tau + \hat{p}_z + \epsilon\hat{p}_\zeta + \hat{\rho}g = -\rho_0 F_V \quad (182)$$

$$-c_p\hat{\rho}_\xi + \epsilon\hat{\rho}_\tau + \tilde{\rho}_z w = G. \quad (183)$$

Introducing (174) into the kinematic interfacial conditions, (164) and (165), gives

$$c_p\eta_\xi - \epsilon\eta_\tau - \left[u^- + \left(u_z^- + \epsilon u_\zeta^-\right)\eta + \frac{1}{2}\left(u_{zz}^- + \epsilon u_{z\zeta}^- + \epsilon^2 u_{\zeta\zeta}^-\right)\eta^2 + \cdots\right]\eta_\xi$$
$$= -\left[w^- + \left(w_z^- + \epsilon w_\zeta^-\right)\eta + \frac{1}{2}\left(w_{zz}^- + \epsilon w_{z\zeta}^- + \epsilon^2 w_{\zeta\zeta}^-\right)\eta^2 + \cdots\right], \quad (184)$$

$$c_p\eta_\xi - \epsilon\eta_\tau - \left[u^+ + \left(u_z^+ + \epsilon u_\zeta^+\right)\eta + \frac{1}{2}\left(u_{zz}^+ + \epsilon u_{z\zeta}^+ + \epsilon^2 u_{\zeta\zeta}^+\right)\eta^2 + \cdots\right]\eta_\xi$$
$$= -\left[w^+ + \left(w_z^+ + \epsilon w_\zeta^+\right)\eta + \frac{1}{2}\left(w_{zz}^+ + \epsilon w_{z\zeta}^+ + \epsilon^2 w_{\zeta\zeta}^+\right)\eta^2 + \cdots\right], \quad (185)$$

The dynamic condition, (173), becomes

$$\left[\hat{p}^- - \hat{p}^+\right]_{z=0} + \left[\left(\hat{p}_z^- - \hat{p}_z^+\right) + \epsilon\left(\hat{p}_\zeta^- - \hat{p}_\zeta^+\right)\right]_{z=0}\eta$$
$$+ \frac{1}{2}\left[\left(\hat{p}_{zz}^- - \hat{p}_{zz}^+\right) + \epsilon\left(\hat{p}_{z\zeta}^- - \hat{p}_{z\zeta}^+\right) + \epsilon^2\left(\hat{p}_{\zeta\zeta}^- - \hat{p}_{\zeta\zeta}^+\right)\right]_{z=0}\eta^2 + \cdots$$
$$+ \frac{1}{2}\tilde{\rho}_0\left[N^{-2} - N^{+2}\right]\eta^2 + \frac{1}{3!}\frac{\tilde{\rho}_0}{g}\left[N^{-4} - N^{+4}\right]\eta^3 + \cdots = 0. \quad (186)$$

5.4 Expand

Consider the Fourier expansions given by

$$\eta = \sum_{m=-\infty}^{\infty} \eta_m(\tau)e^{imk\xi}, \quad (187)$$

$$w^\pm = \sum_{m=-\infty}^{\infty} w_m^\pm(\tau, z, \zeta)e^{imk\xi}, \quad (188)$$

where m is an integer, and k is the horizontal wavenumber.

The operator on the left hand side of (158) becomes

$$L^\pm = \left(-c_p\frac{\partial}{\partial\xi} + \epsilon\frac{\partial}{\partial\tau}\right)^2\left[\frac{\partial^2}{\partial\xi^2} + \left(\frac{\partial^2}{\partial z^2} + \epsilon\frac{\partial^2}{\partial\zeta^2}\right)^2\right] + N^{\pm 2}\frac{\partial^2}{\partial\xi^2}. \quad (189)$$

Using (188) in (158) and separating Fourier components results in

$$L^{\pm}\left(w_m^{\pm}\right) = M_m^{\pm}. \tag{190}$$

The interfacial boundary conditions are

$$c_p \eta_{m\xi} - \epsilon \eta_{m\tau} + w_m^{\pm} = H_m^{\pm}, \tag{191}$$

$$p_m^{+} - p_m^{-} = Q_m, \tag{192}$$

on $z = 0$.

5.5 Linear solution

An incident wave is assumed to propagate with upwards group velocity in the lower layer, impinging upon the interface. The vertical component of velocity for such a wave is

$$w_1^{-} = \alpha A^{-} e^{i\left(k\xi - n^{-} z\right)} + cc, \tag{193}$$

where $A^{-} = A^{-}(\zeta, \tau)$ is the incident wave amplitude, k and n^{-} are the horizontal and vertical wavenumbers, respectively, and cc means complex conjugate. The resulting dispersion relation is

$$c_p^2 = \frac{N^{-2}}{k^2 + n^{-2}}. \tag{194}$$

However, (193) by itself cannot meet the interfacial conditions. A reflected wave as well as a transmitted wave is required. The combination of waves is given by

$$w_1^{-} = \alpha A^{-} e^{i\left(k\xi - n^{-} z\right)} + \alpha K B^{-} e^{i\left(k\xi + n^{-} z\right)} + cc, \tag{195}$$

$$w_1^{+} = \alpha J B^{+} e^{i\left(k\xi - n^{+} z\right)} + cc, \tag{196}$$

where $B^{-} = B^{-}(\zeta, \tau)$ is the reflected wave amplitude, $B^{+} = B^{+}(\zeta, \tau)$ is the transmitted wave amplitude, n^{+} is the vertical wavenumber in the upper layer, and

$$K = \frac{n^{-} - n^{+}}{n^{-} + n^{+}},$$

$$J = \frac{2n^{-}}{n^{-} + n^{+}}.$$

The corresponding displacement of the interface is

$$\eta_1 = i\alpha \frac{1}{kc_p} J\left[Ae^{ik\xi} - A^* e^{-ik\xi} \right], \tag{197}$$

where A is the amplitude of the interface.

5.6 Amplitude equation

The left-hand-side of (190) is

$$L^{\pm} = c_p^2 \frac{\partial^2}{\partial \xi^2}\left(\frac{\partial^2}{\partial \xi^2} + \frac{\partial^2}{\partial z^2} \right) + N^{\pm 2} \frac{\partial^2}{\partial \xi^2}$$
$$\epsilon\left[-2c_p \frac{\partial^2}{\partial \tau \partial \xi}\left(\frac{\partial^2}{\partial \xi^2} + \frac{\partial^2}{\partial z^2} \right) + 2c_p^2 \frac{\partial^4}{\partial \xi^2 \partial z \partial \zeta} \right] + \bigcirc(\epsilon^2). \tag{198}$$

If c_p is chosen to be

$$c_p^2 = \frac{N^{\pm 2}}{k^2 + n^{\pm 2}},$$

and the linear solution is inserted into (190), then the zeroeth order terms in (198) are exactly zero, leaving

$$\epsilon\left[-2c_p \frac{\partial^2}{\partial \tau \partial \xi}\left(\frac{\partial^2}{\partial \xi^2} + \frac{\partial^2}{\partial z^2} \right) + 2c_p^2 \frac{\partial^4}{\partial \xi^2 \partial z \partial \zeta} \right] + \bigcirc(\epsilon^2).$$

The result for the upper layer is

$$\alpha\epsilon i\left[kc_p\left(k^2 + n^{+2} \right) B_\tau^+ + n^+ k^2 c_p^2 B_\zeta^+ \right] 2Je^{i(k\xi - n^+ z)} + \text{cc},$$

to order $\epsilon^2\alpha$. For the lower layer,

$$\alpha\epsilon i\left[kc_p\left(k^2 + n^{-2} \right) A_\tau^- + n^- k^2 c_p^2 A_\zeta^- \right] 2e^{i(k\xi - n^- z)} + \text{cc}$$
$$\alpha\epsilon i\left[kc_p\left(k^2 + n^{-2} \right) B_\tau^- - n^- k^2 c_p^2 B_\zeta^- \right] 2Ke^{i(k\xi + n^- z)} + \text{cc}. \tag{199}$$

The linear terms in the interfacial conditions with $m = 1$ are $\bigcirc(\alpha)$, and do not add to zero, but instead provide a relationship between the incident

wave amplitude and reflected and transmitted wave amplitudes. The nonlinear terms in the interfacial conditions are $\bigcirc(\alpha^2)$, and no choice of ϵ makes the linear and nonlinear terms balance. Hence the nonlinear terms in the interfacial conditions with $m = 1$ are higher order, and the linear conditions apply:

$$A^-\Big|_{\zeta=0} = B^-\Big|_{\zeta=0} = B^+\Big|_{\zeta=0}. \tag{200}$$

The nonlinear terms in the interfacial conditions with $m = 0$ and $m = 2$ both contribute through $w_2^\pm$ and $u_0^\pm$.

The nonlinear terms result in

$$M^\pm = \bigcirc(\epsilon\alpha^2). \tag{201}$$

The nonlinear terms in the interfacial conditions result in

$$H = -2\alpha^2 \frac{n^+}{kc_p} J\left[A^2 e^{i2k\xi} + A^{*2} e^{-i2k\xi}\right] + \bigcirc(\epsilon\alpha^2), \tag{202}$$

$$Q = -4\alpha^2 \rho_0 \frac{n^{-2}}{k^2} K\left[A^2 e^{i2k\xi} + A^{*2} e^{-i2k\xi} - 2AA^*\right] + \bigcirc(\epsilon\alpha^2). \tag{203}$$

The components for $m = 0, 2$ can be extracted by inspection:

$$H_0 = \bigcirc(\epsilon\alpha^2), \tag{204}$$

$$H_2 = -2\alpha^2 \frac{n^+}{kc_p} J\left[A^2 e^{i2k\xi} + A^{*2} e^{-i2k\xi}\right] + \bigcirc(\epsilon\alpha^2), \tag{205}$$

$$Q_0 = 8\alpha^2 \rho_0 \frac{n^{-2}}{k^2} KAA^* + \bigcirc(\epsilon\alpha^2). \tag{206}$$

$$Q_2 = -4\alpha^2 \rho_0 \frac{n^{-2}}{k^2} K\left[A^2 e^{i2k\xi} + A^{*2} e^{-i2k\xi}\right] + \bigcirc(\epsilon\alpha^2). \tag{207}$$

5.6.1 Second harmonic

Equation (190) with $m = 2$ is now

$$L^\pm\Big(w_2\Big) = M_2^\pm, \tag{208}$$

with boundary conditions

$$c_p \eta_{2\xi} - \epsilon\eta_{2\tau} + w_2^\pm = H_2^\pm, \tag{209}$$

$$p_2^+ - p_2^- = Q_2, \tag{210}$$

on $z = 0$.

As the governing equation is homogeneous, the only particular solution is associated with the boundary conditions, and is

$$w_2^{\pm} = \alpha^2 \frac{8n^{-2}}{kc_p(n_2^- + n_2^+)} K\left[A^2 e^{i(2k\xi \mp n_2^{\pm} z)} + A^{*2} e^{-i(2k\xi \mp n_2^{\pm} z)}\right], \tag{211}$$

where

$$n_2^{\pm} = n^{\pm 2} - 3k^2. \tag{212}$$

5.6.2 Mean flow

The wave-induced mean flow is determined using the wave action principles, as outlined by Acheson [1]. The wave energy is

$$E = \frac{1}{2}\rho_0 \left[\overline{u^2 + w^2 + N^2\eta^2}\right], \tag{213}$$

where η is the displacement of a material line. Again, using the linear solutions,

$$E^- = 2\alpha^2\rho_0 \left[\left(\frac{n^{-2} + k^2}{k^2}\right)\left(A^- A^{-*} + K^2 B^- B^{-*}\right) + K\left(A^{-*} B^- e^{i2n^- z} + A^- B^{-*} e^{-i2n^- z}\right)\right], \tag{214}$$

$$E^+ = 2\alpha^2\rho_0 \left(\frac{n^{+2} + k^2}{k^2}\right) J^2 B^+ B^{+*} \tag{215}$$

The mean flow is determined using

$$\rho_0 u_0 = \frac{E}{c_p}. \tag{216}$$

The result is

$$u_0^- = 2\alpha^2 \frac{1}{c_p}\left[\left(\frac{n^{-2} + k^2}{k^2}\right)\left(A^- A^{-*} + K^2 B^- B^{-*}\right) + K\left(A^{-*} B^- e^{i2n^- z} + A^- B^{-*} e^{-i2n^- z}\right)\right], \tag{217}$$

$$u_0^+ = 2\alpha^2 \frac{1}{c_p}\left(\frac{n^{+2} + k^2}{k^2}\right) J^2 B^+ B^{+*} \tag{218}$$

5.6.3 M_1

To leading order, M_1 is

$$M_1^- = -4\alpha^3 k^2 n^{-2}\Big[K^2\Big|B^-\Big|^2\Big(A^- e^{i(k\xi - n^- z)} + A^{-*} e^{-i(k\xi - n^- z)}\Big) + K\Big|A^-\Big|^2\Big(B^- e^{i(k\xi + n^- z)} + B^{-*} e^{-i(k\xi + n^- z)}\Big)\Big], \quad (219)$$

$$M_1^+ = 0. \quad (220)$$

The result is three amplitude equations:

$$i\Big(A_\tau^- + \frac{n^- k c_p}{k^2 + N^{-2}} A_\zeta^-\Big) + 4\frac{k n^{-2}}{c_p(k^2 + n^{-2})} K^2\Big|B^-\Big|^2 A^- = 0, \quad (221)$$

$$i\Big(B_\tau^- - \frac{n^- k c_p}{k^2 + N^{-2}} B_\zeta^-\Big) + 4\frac{k n^{-2}}{c_p(k^2 + n^{-2})} K\Big|A^-\Big|^2 B^- = 0, \quad (222)$$

$$B_\tau^+ - \frac{n^+ k c_p}{k^2 + n^{+2}} B_\zeta^+ = 0. \quad (223)$$

Recognizing that

$$c_g = -\frac{nk}{k^2 + n^2} c_p,$$

Then these amplitude equations are more generally written as

$$i\Big(A_\tau^- - c_g A_\zeta^-\Big) - 4\frac{n^- c_g}{c_p^2} K^2\Big|B^-\Big|^2 A^- = 0, \quad (224)$$

$$i\Big(B_\tau^- - c_g B_\zeta^-\Big) + 4\frac{n^- c_g}{c_p^2} K\Big|A^-\Big|^2 B^- = 0, \quad (225)$$

$$B_\tau^+ + c_g B_\zeta^+ = 0. \quad (226)$$

Note that c_g is the *vertical* group velocity, while c_p is the *horizontal* phase velocity.

5.7 Results

As the nonlinear part of (226) is exactly zero, then (226) is independent, linked to the solution of (224) and 225) only throught the interfacial conditions. Thus (224)-(225) may be treated simultaneously and waves in the upper layer determined separately, if needed. It is also possible to show several constants throughout the motion, for example,

$$\frac{\partial}{\partial \tau}\left(\left|A^{-}\right|^{2}\right)=\frac{\partial}{\partial \tau}\left(\left|B^{-}\right|^{2}\right). \tag{227}$$

and other results.

It is convenient to treat (224)-(225) numerically using the leap-frog method. The results show that the interaction of the incident wave with its relection beneath the interface generates a higher wave amplitude, and corresponding mean flow, u_0. This mean flow does not appear above the interface, and the mean flow is in fact discontinuous at the interface. Further results will be submitted soon to The Journal of Fluid Mechanics.

6 Stability with a jump in stability and velocity

This problem is concerned the dynamics of waves interacting with an interface that has both a jump in velocity as well as a jump in the Brunt-Vaisala frequency. This problem is motivated by recent observations [4] of large amplitude oscillations over Hawaii. The observations remain unexplained, but suggest resonant over-reflection of internal waves. Previous theoretical results of resonant over-reflection indicate a range of wavenumbers where waves will spontaneously be created by a shear flow; no incident wave. These results have appear in an AIAA conference paper [5], and are the subject of further work by a Ph.D. student.

6.1 Governing equations

Assume incompressible flow, and neglect any diffusion. The flow is assumed to be incompressible, inviscid, and two-dimensional. Stratification is present due to the presence of a non-diffusing quantity, and the flow is assumed to be Boussinesq. Without loss of generality, a coordinate system is chosen to be moving with the average velocity of the two layers. In this moving but inertial coordinate system, the speed of the upper layer is U, and the lower layer is $-U$, following Grimshaw [JFM, 1979]. The flow is then governed by the Euler equations in Boussinesq form, the continuity equation, and the equation of incompressibility:

$$\rho_0 \left[\frac{\partial \hat{u}}{\partial t} \pm U \frac{\partial \hat{u}}{\partial x} + \hat{u} \frac{\partial \hat{u}}{\partial x} + w \frac{\partial \hat{u}}{\partial z} \right] = -\frac{\partial \hat{p}}{\partial x}, \tag{228}$$

$$\rho_0 \left[\frac{\partial w}{\partial t} \pm U \frac{\partial \hat{w}}{\partial x} + \hat{u} \frac{\partial \hat{w}}{\partial x} + w \frac{\partial w}{\partial z} \right] = -\frac{\partial \hat{p}}{\partial z} - \hat{\rho} g, \tag{229}$$

$$\frac{\partial \hat{\rho}}{\partial t} \pm U \frac{\partial \hat{\rho}}{\partial x} + \hat{u} \frac{\partial \hat{\rho}}{\partial x} + w \frac{\partial \hat{\rho}}{\partial z} + \frac{d\overline{\rho}}{dz} w = 0. \tag{230}$$

$$\frac{\partial \hat{u}}{\partial x} + \frac{\partial w}{\partial z} = 0, \tag{231}$$

[4] McHugh, J. P., Dors, I., Jumper, G. Y., Roadcap, J. R., Murphy, E. A., and Hahn, D. C., to appear in JGR, 2008.

[5] McHugh, J. P., Paper AIAA-2009-0109, 47th AIAA Aerospace Sciences Meeting, Orlando, FL, January, 2009.

where (u, w) are the velocities in the (x, z) directions, respectively, $\hat{p}$ is the dynamic pressure, ρ_0 is an average (constant) density, $\overline{\rho}(z)$ is the mean density, $\hat{\rho}$ is the density perturbation, and g is the gravitational constant.

6.2 Interfacial conditions

The mean density profile is chosen to be continuous, but have a discontinous first derivative, such that the fluid exists in two semi-infinite layers, each layer having a unique value of the Brunt-Vaisala frequency. The interface between the two layers must satisfy interfacial conditions. There are two types of interfacial conditions on a material line separating two inviscid layers of fluid; kinematic and dynamic. The kinematic condition in an inviscid flow states that the normal velocity of the material line is equal to the normal component of velocity of the fluid. The dynamic condition states that the pressure must be continuous across the material line.

The kinematic conditions are

$$\eta_t - U\eta_x + \hat{u}_1\eta_x = \hat{w}_1, \tag{232}$$

$$\eta_t + U\eta_x + \hat{u}_2\eta_x = \hat{w}_2, \tag{233}$$

which hold on the interface, $z = \eta$, where u_1, w_1 are velocities in the lower layer, u_2, w_2 are velocities in the upper layer, and η is the vertical displacement of the interface.

A primary difficulty is meeting the interfacial conditions on the actual interface, $z = \eta$, without knowing the position of the interface beforehand. This difficulty is treated by expanding all terms in a Taylor series about the mean position of the interface, in the same manner usually used for free surface flow. The kinematic conditions become

$$\eta_t - U\eta_x + \left[\hat{u}_1 + \hat{u}_{1_z}\eta + \frac{1}{2}\hat{u}_{1_{zz}}\eta^2 + \cdots\right]\eta_x = \left[w_1 + w_{1z}\eta + \frac{1}{2}w_{1zz}\eta^2 + \cdots\right], \tag{234}$$

$$\eta_t + U\eta_x + \left[\hat{u}_2 + \hat{u}_{2_z}\eta + \frac{1}{2}\hat{u}_{2_{zz}}\eta^2 + \cdots\right]\eta_x = \left[w_2 + w_{2z}\eta + \frac{1}{2}w_{2zz}\eta^2 + \cdots\right], \tag{235}$$

where the coefficients are now evaluated at the mean position of the interface, $z = 0$.

The dynamic condition is continuity of total pressure, p. Hence

$$p_1 = p_2 \tag{236}$$

on $z = \eta$, where p_1 and p_2 are the pressures in the lower and upper layers, respectively. Consider the incompressible flow model for now, rather than the more restrictive Boussinesq approximation. The total pressure is segmented into the mean and fluctuating parts:

$$p = \tilde{p} + \hat{p}. \tag{237}$$

Expanding (236) in a Taylor series, as before, gives

$$\begin{aligned}
&[\tilde{p}_1 + \hat{p}_1]\Big|_{z=0} + \frac{\partial}{\partial z}[\tilde{p}_1 + \hat{p}_1]\Big|_{z=0}\eta + \frac{1}{2}\frac{\partial^2}{\partial z^2}[\tilde{p}_1 + \hat{p}_1]\Big|_{z=0}\eta^2 + \cdots = \\
&[\tilde{p}_2 + \hat{p}_2]\Big|_{z=0} + \frac{\partial}{\partial z}[\tilde{p}_2 + \hat{p}_2]\Big|_{z=0}\eta + \frac{1}{2}\frac{\partial^2}{\partial z^2}[\tilde{p}_2 + \hat{p}_2]\Big|_{z=0}\eta^2 + \cdots .
\end{aligned} \tag{238}$$

Several terms may be eliminated immediately. Pressure in the absence of motion is continuous, which gives $\tilde{p}_1 = \tilde{p}_2$ at $z = 0$, allowing these terms to be dropped.

Further simplification is obtained using hydrostatic equilibrium,

$$\frac{\partial \tilde{p}_1}{\partial z} = -\tilde{\rho}_1 g, \tag{239}$$

$$\frac{\partial \tilde{p}_2}{\partial z} = -\tilde{\rho}_2 g, \tag{240}$$

where $\tilde{\rho}_1$ and $\tilde{\rho}_2$ are the mean densities in the two layers. The density profile is assumed continuous at the tropopause (although not smooth), implying $\tilde{\rho}_1 = \tilde{\rho}_2$ at $z = 0$. Equations (239) and (240) then result in

$$\frac{\partial \tilde{p}_1}{\partial z} = \frac{\partial \tilde{p}_2}{\partial z} \tag{241}$$

on $z = 0$. These two terms may be dropped from (238).

Furthermore, the second derivative of $\tilde{p}$ is related to the Brunt-Vaisala frequency:

$$\tilde{p}_{zz} = -\tilde{\rho}_z g = -\tilde{\rho}\left[g\frac{\tilde{\rho}_z}{\tilde{\rho}}\right] = +\tilde{\rho}N^2, \tag{242}$$

which holds for each layer. Higher order terms result can be treated in a similar manner. The dynamic interfacial condition may now be written as

$$\begin{aligned}&\left[\hat{p}_1 - \hat{p}_2\right]_{z=0} + \left[\hat{p}_{1z} - \hat{p}_{2z}\right]_{z=0}\eta + \frac{1}{2}\left[\hat{p}_{1zz} - \hat{p}_{2zz}\right]_{z=0}\eta^2 + \cdots \\ &+\frac{1}{2}\tilde{\rho}_0\left[{N_1}^2 - {N_2}^2\right]\eta^2 + \frac{1}{3!}\frac{\tilde{\rho}_0}{g}\left[{N_1}^4 - {N_2}^4\right]\eta^3 + \cdots = 0,\end{aligned} \tag{243}$$

where $\tilde{\rho}_0$ is mean density at the interface.

The restriction to Boussinesq flow merely implies that $\tilde{\rho}$ is now taken as the constant, ρ_0.

6.3 Amplitude equation

Define the following variables:

$$\begin{aligned}\xi &= x - c_p t, &(244)\\ \chi &= \epsilon\left(x - c_g t\right), &(245)\\ \zeta &= \epsilon^2 z, &(246)\\ \tau &= \epsilon^2 t, &(247)\end{aligned}$$

where c_p and c_g are constants to be determined later, and ϵ is a small parameter. Assume all variables depend now on ξ, χ, ζ, τ, and z.

The governing equations become

$$\begin{aligned}\rho_0\left[\left(\pm U - c_p\right)\hat{u}_\xi + \epsilon\left(\pm U - c_g\right)\hat{u}_\chi + \hat{u}\hat{u}_\xi + \epsilon\hat{u}\hat{u}_\chi + \epsilon^2\hat{u}_\tau + w\hat{u}_z + \epsilon^2 w\hat{u}_\zeta\right]& \\ = -\left[\hat{p}_\xi + \epsilon\hat{p}_\chi\right],&\end{aligned} \tag{248}$$

$$\begin{aligned}\rho_0\left[\left(\pm U - c_p\right)w_\xi + \epsilon\left(\pm U - c_g\right)w_\chi + \hat{u}w_\xi + \epsilon\hat{u}w_\chi + \epsilon^2 w_\tau + ww_z + \epsilon^2 ww_\zeta\right]& \\ = -\left[\hat{p}_z + \epsilon^2\hat{p}_\zeta\right] - \hat{\rho}g,&\end{aligned} \tag{249}$$

$$(\pm U - c_p)\,\hat{\rho}_\xi + \epsilon\,(\pm U - c_g)\,\hat{\rho}_\chi + \hat{u}\hat{\rho}_\xi + \epsilon\hat{u}\hat{\rho}_\chi + \epsilon^2\hat{\rho}_\tau + w\hat{\rho}_z + \epsilon^2 w\hat{\rho}_\zeta + \tilde{\rho}_z w = 0, \tag{250}$$

$$\hat{u}_\xi + \epsilon\hat{u}_\chi + w_z + \epsilon^2 w_\zeta = 0, \tag{251}$$

where the positive sign is used for the upper layer, and the negative sign for the lower layer.

Introducing (244) into the kinematic interfacial conditions, (234) and (235), gives

$$\begin{aligned}
&-\Big(U + c_p\Big)\eta_\xi - \epsilon\Big(U + c_g\Big)\eta_\chi + \epsilon^2\eta_\tau \\
&+\left[u_1 + \left(u_{1z} + \epsilon^2 u_{1\zeta}\right)\eta + \frac{1}{2}\left(u_{1zz} + \epsilon^2 u_{1z\zeta} + \epsilon^4 u_{1\zeta\zeta}\right)\eta^2 + \cdots\right]\Big[\eta_\xi + \epsilon\eta_\chi\Big] \\
&= \left[w_1 + \left(w_{1z} + \epsilon^2 w_{1\zeta}\right)\eta + \frac{1}{2}\left(w_{1zz} + \epsilon^2 w_{1z\zeta} + \epsilon^4 w_{1\zeta\zeta}\right)\eta^2 + \cdots\right],
\end{aligned} \tag{252}$$

$$\begin{aligned}
&\Big(U - c_p\Big)\eta_\xi + \epsilon\Big(U - c_g\Big)\eta_\chi + \epsilon^2\eta_\tau \\
&+\left[u_2 + \left(u_{2z} + \epsilon^2 u_{2\zeta}\right)\eta + \frac{1}{2}\left(u_{2zz} + \epsilon^2 u_{2z\zeta} + \epsilon^4 u_{2\zeta\zeta}\right)\eta^2 + \cdots\right]\Big[\eta_\xi + \epsilon\eta_\chi\Big] \\
&= \left[w_2 + \left(w_{2z} + \epsilon^2 w_{2\zeta}\right)\eta + \frac{1}{2}\left(w_{2zz} + \epsilon^2 w_{2z\zeta} + \epsilon^4 w_{2\zeta\zeta}\right)\eta^2 + \cdots\right],
\end{aligned} \tag{253}$$

The dynamic condition, (243), becomes

$$\begin{aligned}
&\Big[\hat{p}_1 - \hat{p}_2\Big]_{z=0} + \left[\left(\hat{p}_{1z} - \hat{p}_{2z}\right) + \epsilon^2\left(\hat{p}_{1\zeta} - \hat{p}_{2\zeta}\right)\right]_{z=0}\eta \\
&+\frac{1}{2}\left[\left(\hat{p}_{1zz} - \hat{p}_{2zz}\right) + \epsilon^2\left(\hat{p}_{1z\zeta} - \hat{p}_{2z\zeta}\right) + \epsilon^4\left(\hat{p}_{1\zeta\zeta} - \hat{p}_{2\zeta\zeta}\right)\right]_{z=0}\eta^2 + \cdots \\
&+\frac{1}{2}\tilde{\rho}_0\Big[{N_1}^2 - {N_2}^2\Big]\eta^2 + \frac{1}{3!}\frac{\tilde{\rho}_0}{g}\Big[{N_1}^4 - {N_2}^4\Big]\eta^3 + \cdots = 0.
\end{aligned} \tag{254}$$

6.3.1 Reduced equations

The governing equations at each order have leading terms that allow the reduction of the equations to one equation operating on the vertical velocity.

The generic form is

$$\rho_0\Big(\mp U + c_p\Big)u_\xi - p_\xi = \rho_0 Q_1, \tag{255}$$

$$\rho_0\Big(\mp U + c_p\Big)w_\xi - p_z - \rho g = \rho_0 Q_3, \tag{256}$$

$$\rho_0\Big(\mp U + c_p\Big)\rho_\xi - \tilde{\rho}_z w = Q_4, \tag{257}$$

$$u_\xi + w_z = Q_5, \tag{258}$$

where the Q's are the collection of terms of lower order that appear in each equation, different for each order. Eliminate p, u, and ρ by cross-differentiated (255) and (256), then substituting with (257) and (258). The result is

$$\Big(\mp U + c_p\Big)^2\nabla^2 w - \frac{\tilde{\rho}_z g}{\rho_0}w = \Big(\mp U + c_p\Big)\Big[Q_{3_\xi} - Q_{1_z}\Big] + \frac{g}{\rho_0}Q_4 + \Big(\pm U + c_p\Big)^2 Q_{5_z}. \tag{259}$$

Defining

$$N^2 = -\frac{\tilde{\rho}_z g}{\rho_0}, \tag{260}$$

Then (259) becomes

$$\Big(\mp U + c_p\Big)^2\nabla^2 w + N^2 w = \Big(\mp U + c_p\Big)\Big[Q_{3_\xi} - Q_{1_z}\Big] + \frac{g}{\rho_0}Q_4 + \Big(\mp U + c_p\Big)^2 Q_{5_z}. \tag{261}$$

6.3.2 Linear stability

The most general form for a disturbance that can meet the interfacial conditions is

$$\begin{aligned} w_{11} &= A_1 e^{i\left(m\xi - n_1 z\right)} + B_1 e^{-i\left(m\xi - n_1 z\right)} \\ &+ C_1 e^{i\left(m\xi + n_1 z\right)} + D_1 e^{-i\left(m\xi + n_1 z\right)}, \end{aligned} \tag{262}$$

$$\begin{aligned} w_{21} &= A_2 e^{i\left(m\xi - n_2 z\right)} + B_2 e^{-i\left(m\xi - n_2 z\right)} \\ &+ C_2 e^{i\left(m\xi + n_2 z\right)} + D_2 e^{-i\left(m\xi + n_2 z\right)}, \end{aligned} \tag{263}$$

where the terms in (262) containing A_1 and B_1 are incident upon the interface from $z = -\infty$, while the terms in (263) containing C_2 and D_2 are incident from $z = +\infty$.

If the incident waves in each layer are supressed, then this linear solution is

$$w_{11} = C_1\,(\xi,\zeta,\tau)\,e^{i\left(m\xi+n_1 z\right)} + D_1\,(\xi,\zeta,\tau)\,e^{-i\left(m\xi+n_1 z\right)}, \tag{264}$$

$$w_{21} = A_2\,(\xi,\zeta,\tau)\,e^{i\left(m\xi-n_2 z\right)} + B_2\,(\xi,\zeta,\tau)\,e^{-i\left(m\xi-n_2 z\right)}. \tag{265}$$

The interfacial conditions result in

$$\Big(U-c_p\Big)C_1 + \Big(U+c_p\Big)A_2 = 0, \tag{266}$$

$$\Big(U-c_p\Big)D_1 + \Big(U+c_p\Big)B_2 = 0, \tag{267}$$

$$n_1\Big(U+c_p\Big)C_1 - n_2\Big(U-c_p\Big)A_2 = 0, \tag{268}$$

$$n_1\Big(U+c_p\Big)D_1 - n_2\Big(U-c_p\Big)B_2 = 0. \tag{269}$$

In matrix form, these are

$$\begin{bmatrix} (U+c_p) & 0 & (U-c_p) & 0 \\ 0 & (U+c_p) & 0 & (U-c_p) \\ n_2(U+c_p) & 0 & -n_1(U-c_p) & 0 \\ 0 & n_2(U+c_p) & 0 & -n_1(U-c_p) \end{bmatrix} \begin{pmatrix} A_2 \\ B_2 \\ C_1 \\ D_1 \end{pmatrix} = 0.$$

Setting the determinant of this matrix to zero results in

$$\Big[n_1(U+c_p)^2 + n_2(U-c_p)^2\Big]^2 = 0, \tag{270}$$

Implying that the quantity inside square brackets is zero. The resulting equation is identical to equation (1.10) of Grimshaw [JPM, 1979], who considered the same problem with constant N throughout.

The governing equation in each layer determine the vertical wave number in each layer:

$$n_1^2 = \frac{N_1^2}{(U+c_p)^2} - m^2, \tag{271}$$

$$n_2^2 = \frac{N_2^2}{(U-c_p)^2} - m^2, \tag{272}$$

Combining (271), (272), and (270) gives

$$(U+c_p)^2\sqrt{\frac{N_1^2}{(U+c_p)^2}-m^2}+(U-c_p)^2\sqrt{\frac{N_2^2}{(U-c_p)^2}-m^2}=0. \qquad (273)$$

There are apparently two modes that satisfy (273), as outlined by Grimshaw [JFM, 1979]. One mode has $c_p = 0$.

Rearrange (273), take a square to eliminate the square root, expand, simplyify, and rearrange to obtain

$$\left(\frac{c_p}{U}\right)^3-\left[\frac{1}{8}\frac{N_1^2-N_2^2}{U^2m^2}\right]\left(\frac{c_p}{U}\right)^2 - \left[\frac{1}{4}\frac{N_1^2+N_2^2}{U^2m^2}-1\right]\left(\frac{c_p}{U}\right)-\left[\frac{1}{8}\frac{N_1^2-N_2^2}{U^2m^2}\right]=0. \quad (274)$$

There are three solutions to this third-order algebraic equation. Note that if N_1 is assumed equal to N_2, then the results of Grimshaw [JFM, 1979] are recaptured.

One of Grimshaw's modes was $c_p = 0$; this is no longer a solution. As a result, the equation does not reduce to a second-order equation, and the results are not so easily obtained. However this same solution exists for a nonzero value of c_p, and corresponds to the unstable mode for the original Helmholtz instability without a density jump. Note that with a density jump, there is a long-wave instability, whatever the velocity difference. This long-wave instability dissappears with the density jump.

6.4 Results from linear stability

The linear results are shown in figures 9 through 11. Figure 9 shows all the roots of (274) for $\frac{N_1}{N_1} = 2$, indicating all three solutions. Note that the lower branch of c_r corresponds to a zero value of c_i, and is analogous to Grimshaws mode with $c = 0$. All of these solutions do not satisfy the radiation conditions. Figure 10 shows the same case, but only shows the modes that do satisfy the radiation conditions.

Figure 11 gives the results with $N_1 = N_2$, identical to the constant N case of Grimshaw [12], shown here for comparison. Grimshaw showed that there are two modes, one with $c = 0$. The second mode can be seen in figure 11. For $\frac{kU}{N} < \frac{1}{2}$, this mode does not satisfy the resonance conditions,

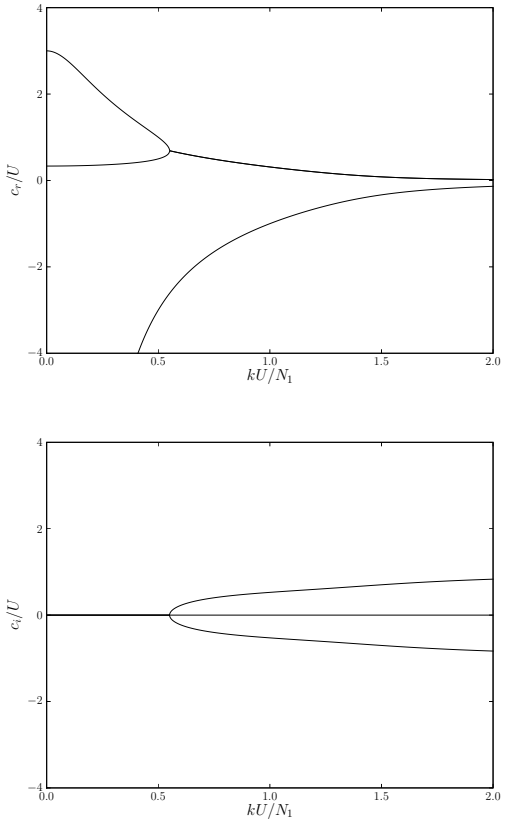

Figure 9: All complex wave speed with $\frac{N_2}{N_1} = 2$

and for $\frac{kU}{N} > \frac{1}{\sqrt{2}}$ this mode is unstable (note the values of c_i). Resonant over-reflection for this mode occurs for $\frac{1}{2} < \frac{kU}{N} < \frac{1}{\sqrt{2}}$.

This same behavior of the second mode exists when N is not constant, as shown in figure 10 for $\frac{N_1}{N_1} = 2$. There is a critical value of $\frac{kU}{N}$ of approximately 0.55 beyond which the flow is unstable. This critical value depends on the ratio $\frac{N_1}{N_1}$. Below this critical value, the results show resonant over-reflection. Note in figure 10 That the lower branch of this second mode extends to $\frac{kU}{N}$ of zero, indicating over-reflection for very long waves. The second mode for constant N does not satisfy the radiation conditions for such long waves, and does not exist. However, the first mode does not exist for $\frac{N_1}{N_1} = 2$, whereas this first mode does exist for all long waves with constant N. Overall, the

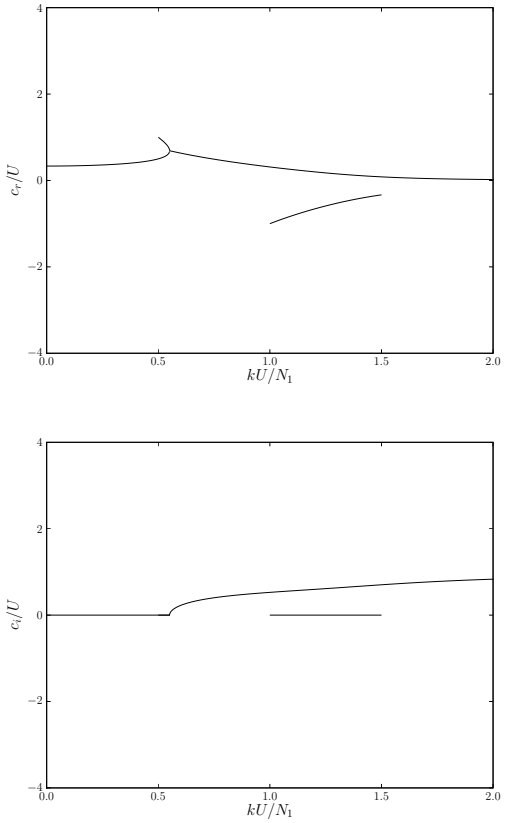

Figure 10: Complex wave speed with $\frac{N_2}{N_1} = 2$

interval of wavenumbers for resonant over-reflection with the sudden change in N is somewhat narrower compared to the case with constant N. Also note that only modes with positive values of c_r exist for the second mode.

A case where N decreases with the vertical is shown in figure 12 for $\frac{N_2}{N_1} = \frac{1}{2}$. For this case, the interval for resonant overreflection is much reduced, as the critical value of $\frac{kU}{N}$ is now approximately 0.275. Furthermore, the wavespeeds for the second mode are all negative, opposite the case with N increasing with the vertical.

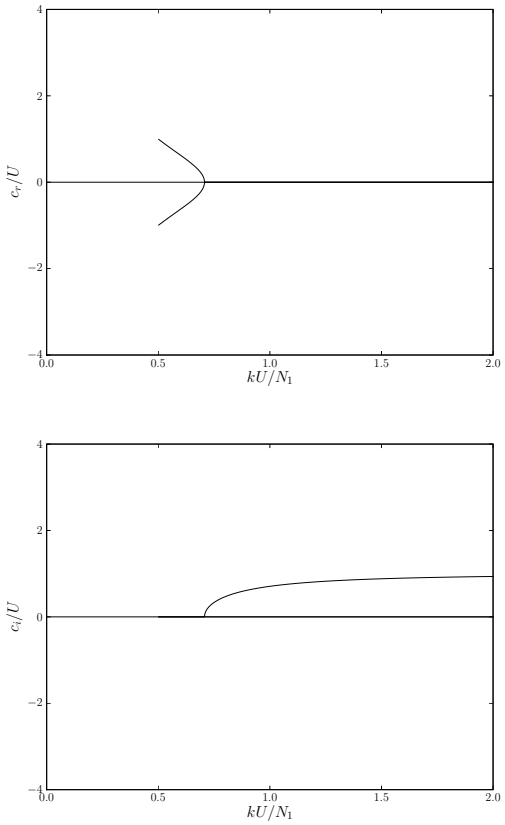

Figure 11: Complex wave speed with $\frac{N_2}{N_1} = 1$

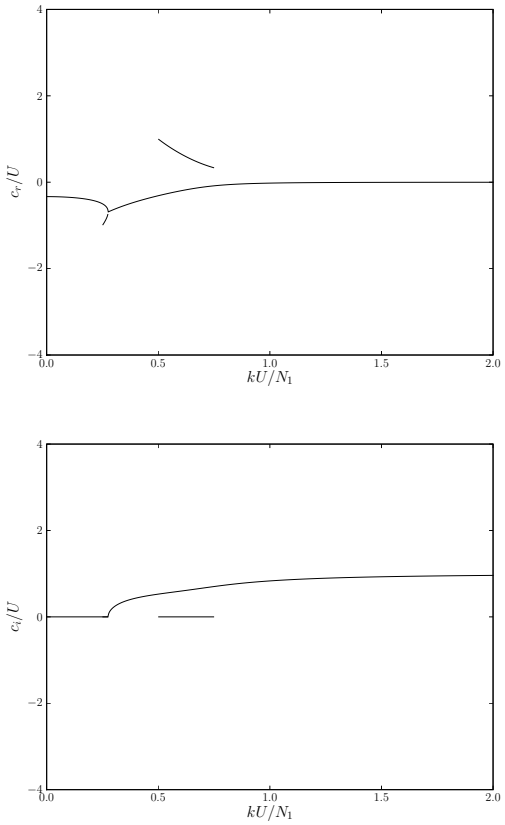

Figure 12: Complex wave speed with $\frac{N_2}{N_1} = \frac{1}{2}$

7 Numerical simulation of mountain waves with rotation

The third continuing task is treating the effects of the Earth's rotation on a field of mountain waves, in collaboration with T. R. Akylas. The work is aimed at verification of a recent theoretical result of Akylas and his associates. The computation is very challenging, as the physical scale of the computation must be very large, to include the mountain wave effects in the far field, yet must also accurately determine the flow directly over the mountain. In order to achieve these disparate scales, a pseudo-three-dimensional approach is employed, where the out-of-plane velocity is non-zero, but does not vary in this third direction. Also, the domain is rectangular, and the mountain is included with an artificial velocity boundary condition. For mountains of small height, the results have accurately reproduced Long's solution. However, A test case is shown in figure (13).

However, as the mountain height is increased to the value where nonlinear effects are important, the artificial boundary condition becomes unstable. A nonlinear version of the boundary condition has been implemented, but also is unstable. Promising results are just now being found with a version of the immersed boundary method.

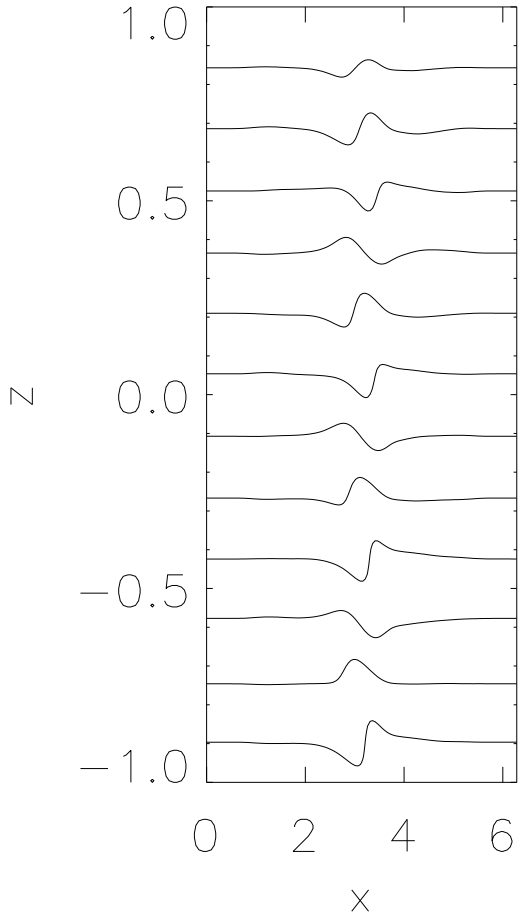

Figure 13: Mountain waves with rotation

8 A vortex pair impinging on the interface

The tropopause is associated with a sudden change in the buoyancy frequency, which is a quantity that is intimately related to internal waves. As a result, the complicated behavior that appears near the tropopause is usually associated with internal waves, and probably usually is driven by internal waves. However, other phenomena can be effect by this sudden change in N, and one important process is considered here: a vortex pair.

The tropopause may be a barrier for turbulence, as well as internal waves, which may account for some of the observations. The simplest case of a turbulent-like flow is a vortex pair. The vortex pair, or vortex ring in three dimensions, will propagate with a fixed speed, raising the question as to whether a vortex pair will reflect off of the tropopause in a manner similar to internal waves.

To investigate this possibility, a vortex pair has been studied numerically. The governing equations are the anelastic equations. The numerical method is an explicit third-order Adams-Bashforth method, spectral in space. The work was performed by a graduate student, Nicolas Jenkins.

8.1 Results

A vortex pair oriented to propagate vertically will move vertically with approximately constant speed. In a viscous flow, the vortex pair gradually loses energy, but maintains it's coherent form. In a stratified flow, a strong vortex pair will act mostly like the constant-density case, however a weak vortex or vortex pair will disintegrate into internal waves very quickly. In a viscous stratified flow, an initially strong vortex pair will act like the constant-density case until the pair has lost some energy, and then the vortex pair will disintegrate into internal waves.

The research considered a relatively strong vortex pair such that the vortex pair retains a coherent form. The pair was released below the interface and allowed to impinge upon it. The results are shown in figure (14) for three time steps, with the top figure the earliest time and the bottom the latest. The top figure shows the vortex pair beneath the interface (shown with the dashed line), the middle figure the pair has passed through the interface, and in the third figure, the pair has returned to the interface. What happens is that the vortex pair is trapped by the interface and winds up oscillating through the interface. Note that in a layer of constant N, the vortex pair

continuous to propaga upward until internal waves are created.

These results show that indeed the tropopause is a filter for certain scales of vortical motion, not just internal waves. It is likely therefore that turbulence is filtered by the tropopause, which may account for some of the observations. These results will soon be submitted to The Journal of Fluid Mechanics.

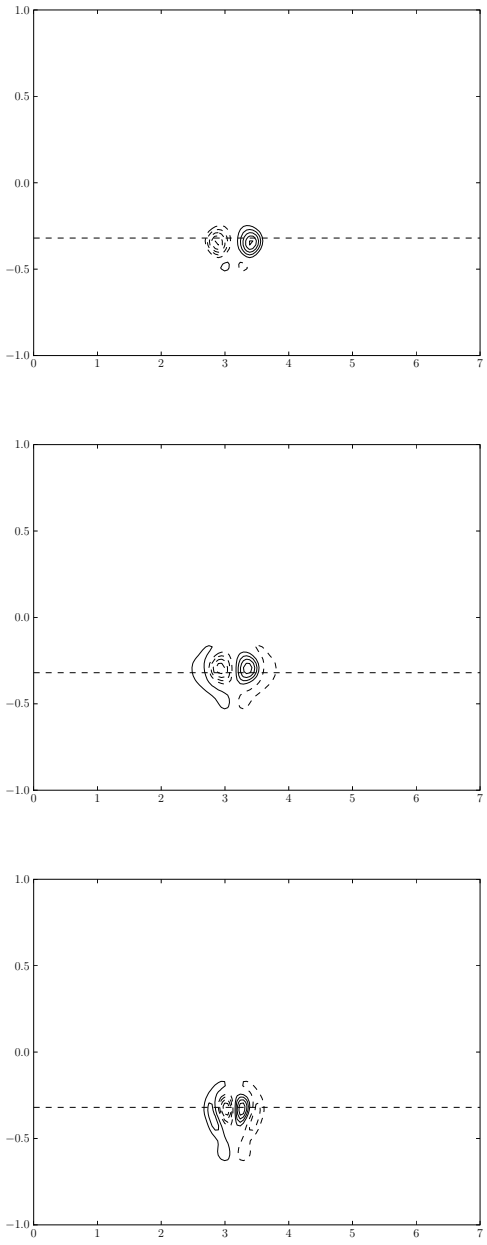

Figure 14: Contours of vorticity at three different times

References

[1] D. J. Acheson, "On over-reflexion," *Journal of Fluid Mechanics*, **77**, pp. 433-472, 1976.

[2] P. S. Anderson, 2004: Using atmospheric solitons to probe the mechanism of interaction between internal waves and a porous surface, Conference on Waves and Turbulence in the Atmosphere, London Institute for Mathematical Sciences.

[3] Andreassen, O., Wasberg, C. E., Fritts, D. C., and Isler, J. R.,: Gravity wave breaking in two and three dimensions 1. Model description and comparison of two-dimensional evolutions. Journal of Geophysical Research, **99**, pp. 8095-8108, (1994).

[4] Bacmeister, J. T. and Schoeberl, M. R.: Breakdown of vertically propagating two-dimensional gravity waves forced by orography. Journal of Atmospheric Science, **46**, pp. 2109-2134, (1989).

[5] T. B. Benjamin, "Internal waves of finite amplitude and permanent form," *Journal of Fluid Mechanics*, **25**, pp. 241-270, 1966.

[6] Boyd, J. P.: Chebyshev and Fourier spectral methods. Dover, (2001).

[7] Craik, A. D. D., 1985: *Wave interactions and fluid flows*. Cambridge University Press.

[8] Durran, D. R., 1992: Two-layer solutions to Long's equation for vertically propagating mountain waves: how good is linear theory? *Quarterly Journal of the Meteorlogical Society*, **118**, 415-433.

[9] Durran, D. R.: Numerical methods for wave equations in geophysical fluid dynamics. Springer, (1998).

[10] Eliassen, A., and E. Palm, 1961: On the transfer of energy in stationary mountain waves. *Geofysiske Publikasjoner*, **XXII**.

[11] D. C. Fritts, "Gravity waves saturation in the middle atmosphere: A review of theory and observation," *Reviews of Geophysics and Space Physics*, **22**, pp. 275-308, 1984.

[12] R. H. J. Grimshaw, "On resonant over-reflexion of internal gravity waves from a Helmholtz velocity profile," *Journal of Fluid Mechanics*, **90**, pp. 161-178, 1979.

[13] Holton, J. R.: An introduction to dynamic meteorology. Academic Press, (1992).

[14] Kim, J., Moin, P., and Moser, R.: Turbulence statistics in fully developed channel flow at low Reynolds number. Journal of Fluid Mechanics, **177**, pp. 133-166, (1987).

[15] Klemp, J. B., and Lilly, D.: Numerical simulation of hydrostatic mountain waves. Journal of the Atmospheric Sciences, **35**, pp. 78-107, (1978).

[16] Lipps, F. B. and Hemler, R. S.: A scale analysis of deep moist convection and some related numerical calculations. Journal of Atmospheric Science, **39**, pp. 2192-2210, (1959).

[17] Long, R. R., 1953: Some aspects of the flow of stratified fluids. I. A theoretical investigation. *Tellus*, **5**, 42-57.

[18] McHugh, J., I. Dors, G. Jumper, J. Roadcap, E. Murphy, and D. Hahn, 2008: Large variations in balloon ascent rate over Hawaii. *Journal of Geophysical Research*, **113**.

[19] Ogura, Y. and Phillips, N. A.: Scale analysis of deep and shallow convection in the atmosphere. Journal of Atmospheric Science, **19**, pp. 173-179, (1962).

[20] Orszag, S. A. and Patera, A. T.: Subcritical transition to turbulence in planar shear flows. Proc. Symp. of The Mathematics Research Center, University of Wisconsin-Madison, **13-15**, pp. 127-146, October, (1980).

[21] Partl, W., 1962: Clear air turbulence at the tropopause levels. *Navigation*, **9**, 288-295.

[22] E. Pelinovsky, O. Polukhina, A. Slunyaev, and T. Talipova, "Internal Solitary Waves," in "Solitary Waves in Fluids," ed. Grimshaw, WIT Press, 2007.

[23] Rayleigh, J. W. S.: The theory of sound. Volume Two. Dover, 1945.

[24] Renfrew, I. A., and P. S. Anderson, 2006: Profiles of katabatic flow in summer and winter over Coats Land, Antarctica. *Quarterly Journal of the Royal Meteological Society*, **132**, 779-802.

[25] V. Sivakumar, P. B. Rao, and H. Bencherif, "Lidar observations of middle atmospheric gravity wave activity over a low-latitude site (Gadanki, 13.5° N, 79.2° E)," *Ann. Geophy.*, **24**, pp. 823-834, 2006.

[26] S. A. Smith, D. C. Fritts, and T. E. VanZandt, "Evidence for a saturated spectrum of atmospheric gravity waves," *Journal of the Atmospheric Sciences*, **44**, pp. 1404-1410, 1987.

[27] Solomonoff, A. and Turkel, E.: Global collocation methods for approximation and the solution of partial differential equations. Icase report no. 86-60, (1960).

[28] Stokes, G. G., 1847: On the theory of oscillatory waves. *Transactions of the Cambridge Philosophical Society*, **8**, 441-455.

[29] Sutherland, B. R.: Finite-amplitude internal wavepacket dispersion and breaking. Journal of Fluid Mechanics, **429**, pp. 343-380, (2001).

[30] Thorpe, S. A., 1968: On the shape of progressive internal waves. *Proceeding of the Royal Society A*, **263**, 563-614.

[31] Van Zandt, T. E., and Fritts, D. C.: A theory of enhanced saturation of the gravity wave spectrum due to increases in atmospheric stability. Pure and Applied Geophysics, **130**, pp. 399-420, (1989).

[32] Vandeven, H.: Family of spectral filters for discontinuous problems. Journal of Scientific Computing, **6**, pp. 159-192, (1991).

[33] Waltersheid, R. L. and Schubert, G.: Nonlinear evolution of an upward propagating gravity wave: overturning, convection, transience, and turbulence. Journal of Atmospheric Science, **47**, pp. 101-125, (1990).

[34] Wilhelmson, R. and Ogura, Y.: On the pressure perturbation and the numerical modeling of a cloud. Journal of Atmospheric Science, **29**, pp. 1295-1307, (1959).

[35] Wolff, J. K., and R. D. Sharman, 2008: Climatology of upper-level turbulence over the contiguous United States. *Journal of Applied Meteorology and Climatology*, **47**, 2198-2214.

[36] Yih, C. S., 1974: Progessive waves of permanent form in continuously stratified fluids. *Physics of Fluids*, **17**, 1489-1495.